Mineral magnetic characterization of the Upper Pleniglacial Nussloch loess sequence (Germany): an insight into local environmental processes

Samuel N. Taylor,[1] France Lagroix,[1] Denis-Didier Rousseau[2,3] and Pierre Antoine[4]

[1]*Institut de Physique du Globe de Paris, Sorbonne Paris Cité, Univ Paris Diderot, UMR7154 CNRS, 1 rue Jussieu, F-75005 Paris, France.*
E-mail: taylor@ipgp.fr
[2]*Ecole Normale Supérieure, Laboratoire de Météorologie Dynamique, UMR8539 CNRS & CERES-ERTI, 24 rue Lhomond, F-75005 Paris, France*
[3]*Lamont-Doherty Earth Observatory of Columbia University, Palisades, NY 10964, USA*
[4]*Laboratoire de Géographie Physique, Environnements quaternaires et actuels UMR8591 CNRS-Univ. Paris I-UPEC, 1 place Aristide Briand, F-92195 Meudon, France*

SUMMARY: MINERAL MAGNETIC ANALYSIS OF THE NUSSLOCH LOESS SEQUENCE

(1) First comprehensive environmental magnetism study of the Nussloch (Rhine River Valley, Germany) loess/palaeosol deposit.

(2) Bulk ferrimagnetic concentration parameters are dominantly controlled by variations in coarse-grained MD ferrimagnetic particles of detrital aeolian origin.

(3) The imprint of waterlogging-induced redoxomorphic processes on the magnetic record is observed by dissolution of fine-grained magnetic minerals.

(4) The interpretation of magnetic susceptibility variations alone within loess and palaeosol deposits following the wind-vigour or pedogenic enhancement models will be hindered by waterlogging-induced redoxomorphic processes, if present.

SUMMARY

Presently, most loess/palaeosol magnetic susceptibility records are interpreted as following either the wind-vigour model or the pedogenic enhancement model. However redoxomorphic processes induced by waterlogging, often referred to *gleying* in the loess literature, are also known to alter loess deposits but their impact on loess/palaeosol magnetic susceptibility records has received little attention. The reported rock magnetic study aims to characterize the mineral magnetic response of loess to waterlogging-induced redoxomorphic processes, thus improving our understanding of mineral magnetic changes within loess deposits with respect to environmental and climate conditions. The Nussloch loess-palaeosol deposit (Rhine Valley, Germany) was targeted because it is one of the best-studied Pleniglacial deposits for Western Europe in which numerous tundra gley intervals have been identified. Moreover, a comprehensive high-resolution environmental magnetism study has never been undertaken for this site.

Various rock magnetism experiments were conducted at both room and low temperatures to characterise the composition, concentration and relative magnetic grain size of the mineral magnetic assemblage. The relative changes in magnetic parameters within the investigated loess interval are primarily controlled by (1) varying concentrations of coarse-grained ferri-magnetic particles of detrital (aeolian) origin and (2) dissolution of fine-grained ferrimagnetic particles related to *in situ* post-depositional alteration promoted by waterlogging-induced redoxomorphic processes. Goethite is found to be ubiquitous throughout the studied interval and is argued to have both a primary (aeolian) and secondary (*in situ*) origin. We conclude, that redoxomorphic processes induced by waterlogging, if present, will hinder the interpretation of magnetic susceptibility variations within loess and palaeosol deposits following the expected relationships dictated by the wind-vigour and the pedogenic enhancement magnetism models.

Key words: Environmental magnetism; Rock and mineral magnetism; Europe.

1 INTRODUCTION

Comparisons between marine, ice core and continental records of past climates can improve the understanding of the Earth's global climate system. Evidence of millennial-scale climate variations during the last glacial period has been found from both ice and marine cores (e.g. Dansgaard *et al.* 1993; Bond *et al.* 1997; McManus *et al.* 1999). However terrestrial records are often unavailable, due to a relative sparsity of material, to formulate a robust coupling between the continental and marine climate. In that context, loess deposits have become one of the most important terrestrial archives for palaeoclimate research (e.g. Kukla 1975; Heller & Evans 1995; Antoine *et al.* 2001; Derbyshire 2001; Haesaerts *et al.* 2003; Haase *et al.* 2007)

Since the pioneering work of Heller & Liu (1982, 1986), rock magnetic studies of loess-palaeosol deposits have been used for palaeoclimatic and chronological research (e.g. Matasova *et al.* 2001; Spassov *et al.* 2003; Lagroix & Banerjee 2004a,b; Wang *et al.* 2006; Jordanova *et al.* 2007; Geiss *et al.* 2008; Maher *et al.* 2010; Necula *et al.* 2013). Rock magnetic studies on Chinese loess have shown it is possible to retrieve palaeoclimatic signals from rock magnetic proxies (e.g. review by Liu *et al.* 2007), albeit a universal model remains elusive. It is generally observed across the Chinese Loess Plateau that palaeosols have higher values of magnetic susceptibility (χ) with respect to loess, while there is an increasing trend in this value from northwest to southeast. This increase is attributed to the pedogenic production of ultrafine magnetic particles, given rise to the pedogenic enhancement model, which in turn has been linked to palaeoprecipitation and the strength of the SE Asian summer monsoon (Heller *et al.* 1993; Maher *et al.* 1994; Porter *et al.* 2001). In Europe, topsoils developing on loess and their intercalated palaeosols are in general, magnetically enhanced with respect to the parent material [e.g. Dolni Vestonice, Czech Republic (Oches & Banerjee 1996); St. Pierre-les-Elboeuf, France (Antoine *et al.* 1999); Mostistea, Romania (Panaiotu *et al.* 2001); Roxolany, Ukraine (Gendler *et al.* 2006); Viatovo, Bulgaria (Jordanova *et al.* 2007); Batajnica/Stari Slankamen, Serbia (Marković *et al.* 2009, 2011; Buggle *et al.* 2014)]. However, the environmental significance and/or control on magnetic enhancement observed across European deposits, similar to efforts in the U.S. Great Plains (Geiss & Zanner 2007) has yet to be proposed, inhibiting the development of a potential regional magnetism based palaeoprecipitation reconstruction. In Central Alaskan deposits, the magnetic susceptibility of the loess is greater than that of the palaeosols. Stronger winds during glacial times can transport dense iron oxide particles more efficiently than weaker winds during interglacial times resulting in a higher concentration of iron oxides and therefore higher magnetic susceptibility in loess with respect to palaeosols (Béget *et al.* 1990). This observation leads to the proposed loess wind-vigour model (Evans 2001) and anisotropy of magnetic susceptibility studies to the reconstruction of palaeowind directions (Lagroix & Banerjee 2002, 2004b). It has also been suggested that low values of magnetic susceptibility observed within palaeosols in central Alaska, Europe and Siberia could be a reflection of post-depositional alteration associated with waterlogging (Nawrocki *et al.* 1996; Liu *et al.* 1999; Zhu *et al.* 2003; Orgeira *et al.* 2011; Baumgart *et al.* 2013).

The response of the magnetic mineral assemblage in loess and palaeosols to waterlogging-induced redoxomorphic processes, commonly referred to *gleying* in the loess literature, has received little attention. Yet, to fully develop the use of loess magnetism as a tool for interpreting climate and environmental changes (see review by Liu *et al.* 2012) the impact of other processes, besides

pedogenesis, on the magnetic record must be more comprehensively understood. To this end, the extensively analysed Weichselian Upper Pleniglacial loess sequences from Nussloch, Germany, where high sedimentation rates and a stratigraphy punctuated by numerous tundra gley horizons are targeted herein (see Antoine *et al.* 2001, 2009; Rousseau *et al.* 2002, 2007; Hatté & Guiot 2005; Moine *et al.* 2005, 2008). To our knowledge, a comprehensive rock magnetic study of the Nussloch sequences has never been undertaken. The goal is therefore to perform a high-resolution and detailed rock magnetic study of the well-known Nussloch loess sequence, focusing on the magnetic mineral assemblage through tundra gley horizons in comparison to that observed in loess horizons. This will improve our understanding of the mineral magnetic response of loess to waterlogging-induced redoxomorphic processes, their impact on the loess/palaeosol magnetic records and ultimately our interpretation of loess magnetism with respect to changing environmental and climate conditions.

2 SETTING AND BACKGROUND

The Nussloch sections are exposed within an active quarry, located on the southern fringe of the Odenwald plateau near the right bank of the Rhine valley approximately ten kilometres south of Heidelberg in Germany (49°18′59″N; 8°43′54″E; Fig. 1). The sections lie on the Eastern side of the Upper Rhine Graben where loess (wind-blown dust with grain size dominated by the silt fraction) has been deposited in 'a series of large dune-like structures known as Gredas, oriented in a northwest to southeast direction' (Antoine *et al.* 2001; Rousseau *et al.* 2007). The source of this dust is thought to be both local and regional, with fine components from the NW European continent (English Channel and North Sea basin) and coarser material from a nearby periglacial, braided alluvial plain of the river Rhine (Lautridou 1985; Sima *et al.* 2009). Preliminary lead isotope and rare earth elements studies from the silt fraction indicate a local source for carbonate and allochthonous silicates (Rousseau *et al.* 2002).

The sedimentology and pedostratigraphy of the Nussloch loess-palaeosols deposit is first described in Antoine *et al.* (2001, 2009). The P4 sequence (Fig. 2) is one of a series of profiles within the quarry that reveal a Weichselian loess and palaeosol sequence (Antoine *et al.* 2002, 2009). This sequence covers the last glacial
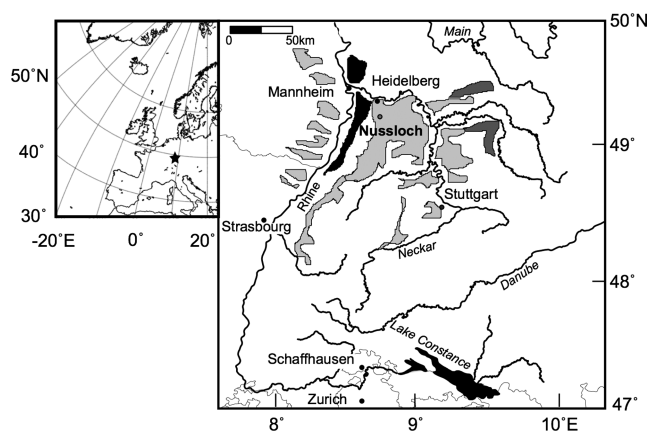

Figure 1. Location map of the Nussloch sequences (star) in relation to Western Europe. The inset map shows the location with respect to regional drainage and loess deposits (light grey = loess, dark grey = loess derivate and black = aeolian sand based on the high resolution map by Haase 2007). Main river channels and cities are highlighted.
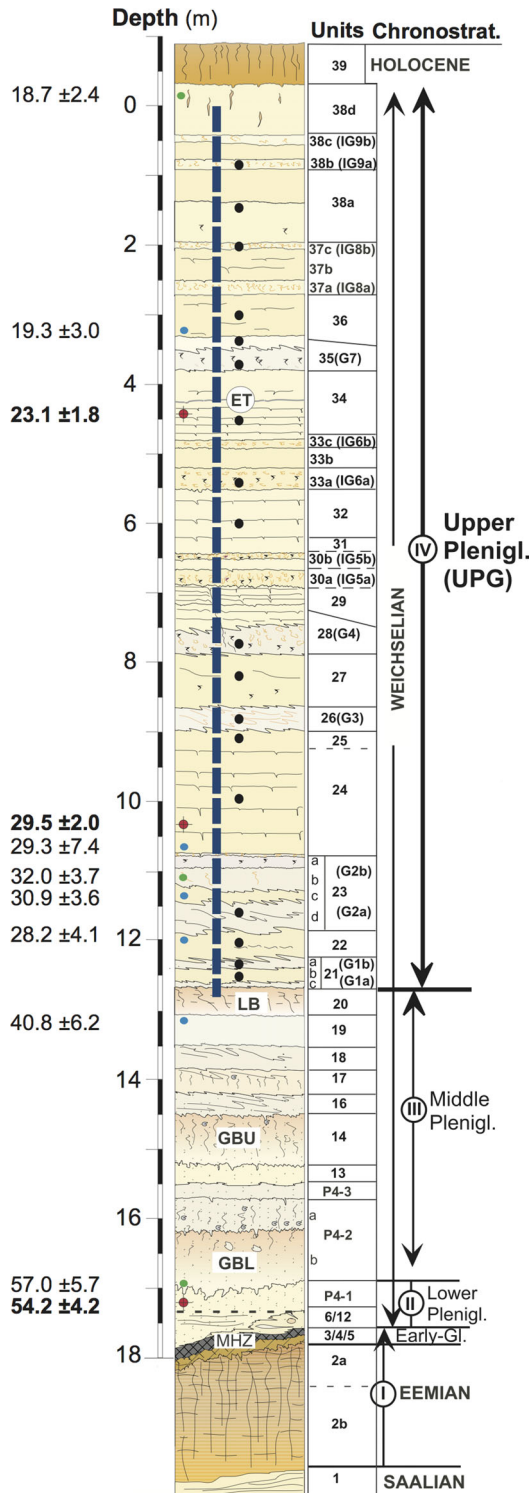
Figure 2. Stratigraphy of the Nussloch P4 profile (original version with full description in Antoine *et al.* 2009). The samples in this study are shown by the central blue column, the older section of the profile is added for completeness. ET, Eltviller Tuff; LB, Lohner Boden (arctic brown soil); GB, Graselberger Boden (Upper and Lower boreal brown soils); MHZ, Mosbacher Humus Zone. G1–G7 main tundra gley horizons IG5–IG9: weak (incipient) tundra gley horizons. Black circles mark the representative samples characterized by low temperature magnetism. Blue and green circles show the sampling depth of IRSL age determinations published in Rousseau *et al.* (2007) and Bibus *et al.* (2007), respectively. Red circles show depths sampled for OSL age determination on quartz grains (Tissoux *et al.* 2010).

cycle and has a thickness of about 18 m. The top 13 m below the topsoil was deposited between 37 000 and 18 000 yr ago, according to a range of infrared and optically stimulated luminescence age determinations (Lang *et al.* 2003; Bibus *et al.* 2007; Rousseau *et al.* 2007; Tissoux *et al.* 2010). A recent study by Kadereit *et al.* (2013) includes a new set of radiocarbon ages and suggests a re-evaluation of the chronology at Nussloch, especially the position of the Lohner Boden soil to a younger period of formation than previously interpreted. Based on the age model presented in Rousseau *et al.* (2007) and Antoine *et al.* (2009), the sedimentation rates for the 13–0 m depth interval average to 1 mm per year resulting in a dilated stratigraphy for the 37–18 kyr period. If one considered the age model presented in Kadereit *et al.* (2013), sedimentation rates would be even greater. Markedly higher sedimentation rates are nevertheless likely during the deposition of the main laminated loess section, which exhibit 2–5 mm individual fining upward layers (Antoine *et al.* 2002). The dominantly unimodal grain size distribution above the Lohner Boden (LB: arctic brown palaeosol; Fig. 3) suggests the sedimentological grain size is controlled by transport mechanisms (Vandenberghe 2013).

The 0 m line of the profile is fixed approximately one metre below the present-day surface (Unit 38d in Fig. 2) where depths increase down profile with the 18 m mark just above the Eemian palaeosol. The upper 13 m section, containing loess layers and tundra gley horizons as the main stratigraphic components (Antoine *et al.* 2009), can be divided into three parts: *Base*) ∼13–11 m showing several homogeneous calcareous loess units and cryoturbated tundra gley horizons, *Middle*) ∼11–4 m showing upward-fining laminated, calcareous loess with cryo-dessication microcracks and cryoturbated tundra gleys, *Top*) ∼4–0 m consists of homogeneous loess and incipient tundra gley horizons including a tephra layer (Juvigné & Semmel 1981; Pouclet & Juvingé 2009). The stratigraphic intervals identified as tundra gley or incipient tundra gley are defined from field observation of discoloration of the loess to greyish and greenish hews and the presence of reddish banding or staining. While the upper boundary of tundra gley horizons is often very distinct, in the field, the lower boundary is much more diffuse. However, higher total organic carbon (TOC) content, weak decalcification and carbonate precipitation as <1 cm hard nodules observed at the base of tundra gley horizons have lead Antoine *et al.* (2001, 2009) and later Gocke *et al.* (2013) to interpret these intervals as tundra gley or incipient tundra gley soil horizons. No observable differentiation can be made at the thin section scale between a tundra gley and loess intervals.

The observed discolouration within tundra gley horizons are a result of waterlogging and are associated with slight increases in surface moisture, a consequence from enhanced seasonal melting of the active layer and snowpack thawing (Evans & Heller 2003; Antoine *et al.* 2009). As such, waterlogged conditions favour redoxomorphic reactions and may lead to a diagenetic alteration of the sediment and does not intrinsically lead to the formation of a soil or pedogenic alteration of the sediment. This does not exclude the action of both redoxomorphic processes induced by waterlogging and soil forming processes within the same horizon as is observed at Nussloch and reported above. Observations of terrestrial, hygrophilous mollusc faunas in tundra gley horizons are indicative of a development in biological activity, suggesting a wetter climate (Moine *et al.* 2008). Finally, organic geochemistry highlighted only C3 plants with $\delta^{13}C$ values ranging between –23.5‰ and –25‰ (Hatté *et al.* 1999) and *n*-alkane biomarkers suggest the absence of deciduous trees and shrubs during the period of loess accumulation considered herein (Zech *et al.* 2012).
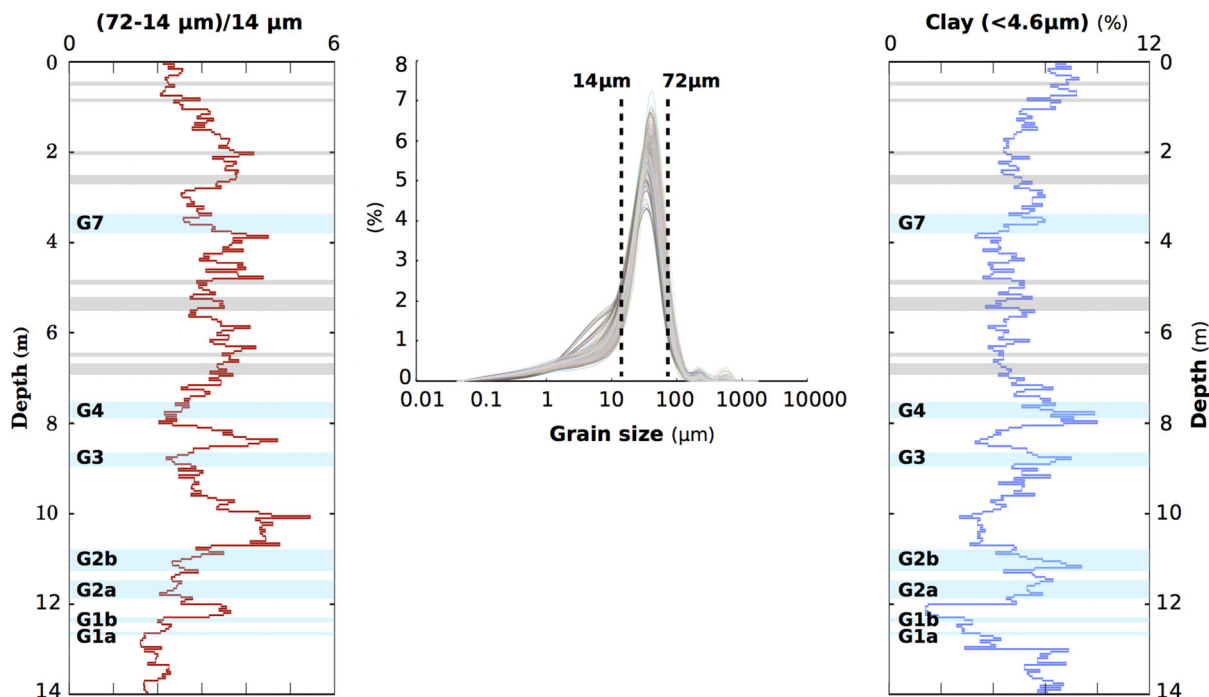
Figure 3. Granulometry data (continuous 5 cm sampling interval) for the Nussloch profile P4 determined using a laser particle sizer and calibrated using the classical pipette method (see Antoine *et al.* 2009) Left-hand panel: grain size ratio (coarse silt to fine silt). Centre panel: Grain size distribution between 14 and 0 m displaying the dominantly unimodal distribution. Right-hand panel: fine grain size fraction (clay percentage).

During the latter stages of the review process of the present manuscript, Gocke *et al.* (2014) published a multiproxy study of a Nussloch profile located on the western edge of the quarry some 500 m west of P4. Limited rock magnetic data (χ, frequency dependence of χ (χ_{fd}), and *S*-ratio) are presented at a low resolution (20 cm sampling interval over 77 per cent of the sequence) for a profile spanning from the Holocene top soil to late stages of the lower Pleniglacial. They argue for important destruction and transformation of detrital ferrimagnetic particles in both loess and paleosols underlying the Holocene soil based on an observed linear increase in χ_{fd} with decreasing χ. Otherwise, the closest rock magnetic study site to Nussloch was provided by Terhorst *et al.* (2001); a loess-palaeosol sequence situated between Nussloch and Maisbach in SW Germany. However, only the magnetic susceptibility data is fully discussed resulting in only a limited interpretation. Terhorst *et al.* (2001) observe low values of magnetic susceptibility in unweathered loess units and high values in palaeosols similar to the reported susceptibility profiles herein and for other Nussloch sequences (Antoine *et al.* 2001, 2009; Bibus *et al.* 2007; Gocke *et al.* 2014). Baumgart *et al.* (2013) investigated three loess deposits in the Saxony region of Eastern Germany. They report hydromorphic solifluction, waterlogging and gleying in the Eemian palaeosol (denoted S1) and the overlying palaeosols (Hz and fG), respectively. They observe low magnetic susceptibility, low anhysteretic remanent magnetization (ARM), low *S*-ratio and frequency dependence of magnetic susceptibility up to 6 per cent (Baumgart *et al.* 2013; their fig. 10). They conclude that these palaeosols underwent 'formation of hard magnetic minerals in addition to a strong reduction in the relative abundance of primary detritic or pedogenic MD and SD grains' due to reworking and waterlogging.

There have been several proposed links between North Atlantic climate events deduced from Greenland ice cores and certain characteristics of this sequence, predominantly the correlation between the Greenland dust records and the variations in loess grain size

parameters. First, it has been proposed that various Dansgaard-Oeschger (D-O) events are recorded within these sediments, with warm phases of the D-O events corresponding to the development of tundra gley horizons and underlying soils (Rousseau *et al.* 2002, 2007; Hatté & Guiot 2005; Moine *et al.* 2008; Antoine *et al.* 2009). Secondly, the possibility of recording events coeval to Heinrich (H) stadials and these types of deposits has been investigated. The impact of Heinrich stadials on the malacofauna cannot be directly identified (Moine *et al.* 2008) however, periods of coarse sediment deposition (i.e. increased aeolian dynamics) are observed to be penecontemporaneous with Heinrich stadials (Antoine *et al.* 2009).

3 SAMPLING AND MEASUREMENTS

The top 13 m of the P4 sequence, terminating 1m below the surface, was sampled continuously in the field within aluminium bars 50 cm in vertical length, 4.5 cm in width and 3 cm in depth. In the laboratory, these were subsampled every 2 cm, with each interval homogenized and packed into plastic boxes ($\sim$7–8 g bulk subsample) and gelcaps ($\sim$0.3–0.4 g bulk subsample) complying with the specification of the various apparatus used. Assuming a constant sedimentation rate through the loess interval, each subsample represents an approximate 20-yr period of deposited material.

Low field magnetic susceptibility (χ_{bulk}) of each subsample was measured using a Kappabridge KLY-2. Hysteresis and backfield analyses were measured on the gelcaps using a Princeton Measurements Vibrating Sample Magnetometer (μ-VSM) within the IPGP-IMPMC Mineral Magnetism Analytical Platform. Hysteresis loops were measured in a maximum field of $\pm$1.5 T. The ferrimagnetic susceptibility (χ_{ferri}) was calculated by subtracting the high field slope (χ_{hifi}) of the uncorrected hysteresis loops from χ_{bulk}. Saturation magnetization (M_S), saturation remanent magnetization (M_{RS}) and coercive force (B_C) are derived from the corrected

hysteresis loop. Coercivity of remanence (B_{CR}) is determined from the reverse field needed to reduce M_{RS} to zero. S-ratios were calculated from the backfield data by:

$$S_{backfield} = \frac{-(IRM_{backfield})}{SIRM_{1T}}, \tag{1}$$

where IRM is the isothermal remanent magnetization acquired by applying a field in steps of 100 mT and SIRM is the saturation isothermal remanent magnetization. 'Hard' isothermal remanent magnetization (HIRM) was calculated following Thompson & Oldfield ([1986](#)) by:

$$HIRM = 0.5(IRM_{1T} + IRM_{-300\,mT}). \tag{2}$$

ARM was acquired using an LDA-3 AF-Demagnetizer and by applying a decaying alternating field from a peak of 100–0 mT superimposed by a constant DC field of 0.05 mT. The acquired ARM was measured using a 2G DC SQUID cryogenic magnetometer.

Low temperature behaviour was characterized for selective samples using a Quantum Design EverCool Magnetic Properties Measurement System (MPMS-XL5-EC). Three temperature dependence of remanence experiments were conducted. First, samples were given a 2.5 T SIRM at room temperature (RT-SIRM), cooled to 10 K and warmed back to 300 K. This experiment is referred to as RT-SIRM cooling and warming curves. Secondly, samples were cooled in zero-field (ZFC < 0.5 μT) from 300 to 10 K where they acquired a 2.5 T SIRM and on reheating, the acquired low temperature SIRM (LT-SIRM) was measured. Thirdly, a repeat of the previous but with 2.5 T in-field cooling (FC). The experiment combining the last two steps is referred to as ZFC-FC warming curves.

4 RESULTS

The results are split into their experimental categories, with bulk magnetic susceptibility presented first, followed by hysteresis parameters, laboratory remanence experiments and low temperature experiments. Each subsection describes the major variations observed and mean differences between loess layers and tundra gley horizons as they were identified and defined from field observations (see Section 2 and Fig. 2).

4.1. Magnetic susceptibility

The representitivity of the two sub-sampling methods (gelcap and plastic box) was tested from χ_{bulk} measurements (Fig. 4). This is required because certain interparametric ratios are determined from parameters measured on different subsamples (e.g. ARM/IRM) and the mass of the gelcap subsamples (mass = 0.370 ± 0.024 g) are half of a percent of that of the box subsamples (mass = 7.69 ± 0.26 g). The linear correlation demonstrated in Fig. 4 has a slope of nearly one (linear curve fit $\chi^2 = 2 \times 10^{-14}$, $R^2 = 0.92$, Student's t-test correlation probability of 0.96) demonstrating that smaller gelcap subsamples (mean χ_{bulk} = 1.15 ± 0.20 × 10⁻⁷ m³kg⁻¹) are representative of the larger box subsamples (mean χ_{bulk} = 1.13 ± 0.20 × 10⁻⁷ m³kg⁻¹; Fig. 4). This is expected given that both the nature of the aeolian sediment and the sample preparation favour homogenization.

Test measurements ($n = 91$) on a dual-frequency Bartington MS2 probe resulted in Δχ values less than 1 per cent of χ_{bulk}, which is below the detection limit of frequency dependence of the MS2 probe. Additional measurements ($n = 28$) were conducted on an MPMS in an AC field of 160 A m⁻¹ over three to five frequencies
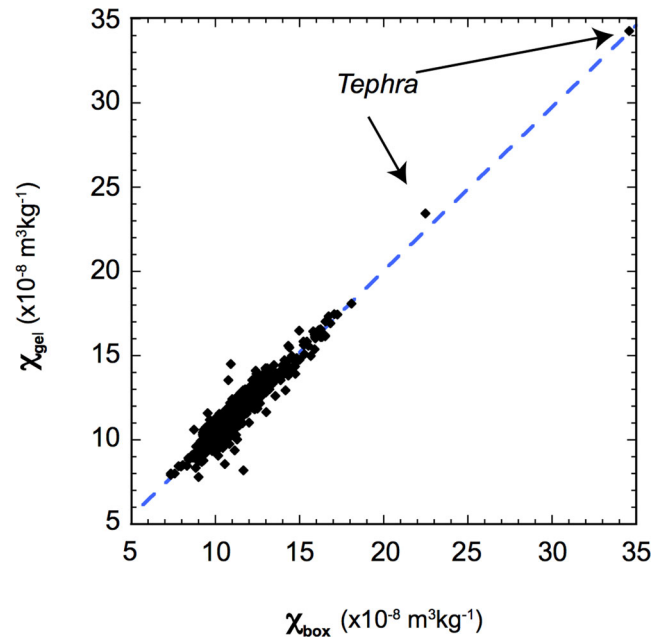

Figure 4. Correlation between the low-field magnetic susceptibility (χ_{bulk}) measured on the bulk higher mass box subsample and lower mass gelcaps subsample specimens (value of $R^2 = 0.923$).

between 10 and 1000 Hz. Three measurements were performed at each frequency defining a measurement mean and standard deviation. The test samples all showed frequency independence of their AC magnetic susceptibility within measurement standard deviation. An absence of superparamagnetic (SP) grains at room temperature through the interval studied is concluded from these tests.

χ_{bulk} values are fairly low (mean for loess samples = $1.16 \pm 0.17 \times 10^{-7}$ m³kg⁻¹) compared to values found in other loess profiles (see review papers Evans & Heller [2001](#); Liu *et al.* [2007](#)). Values and variations with depth of χ_{bulk} (Fig. 5) in this study are very similar to those observed by Bibus *et al.* ([2007](#)), Antoine *et al.* ([2001](#), [2009](#)) and Gocke *et al.* ([2014](#)) for other Nussloch loess sequences. From 13 to 11 m, χ_{bulk} values show large-amplitude fluctuations with a range of approximately 1.0×10^{-7} m³kg⁻¹ (Fig. 5). Between tundra gley unit 2b (G2b at ∼11 m) and 4 (G4 at ∼8 m), the mean value of χ_{bulk} is greater (Fig. 5) at level of $1.29 \pm 0.10 \times 10^{-7}$ m³kg⁻¹ inferring either a relative increase in concentration of magnetic minerals, in ferrimagnetic particle domain size (excluding SP) or in the ratio of magnetically soft to hard minerals. Values remain fairly constant ($\chi_{bulk} = 1.06 \pm 0.07 \times 10^{-7}$ m³kg⁻¹) in the top half of the profile (Fig. 5). This suggests no major changes in both the composition of the input material or any post-depositional alteration. Generally, the tundra gley horizons have lower χ_{bulk} values than their respective underlying loess, although this observation is more complex in the lower three metres of the profile (Fig. 5).

4.2 Hysteresis

The shapes of the hysteresis loops are very homogeneous across the studied section, closing at fields above 400–500 mT and characterized by a narrow width. The two tephra-containing samples show the same shape, only with a stronger magnetization. From uncorrected hysteresis loops, χ_{hifi} is subtracted from χ_{bulk} to quantify χ_{ferri}. The paramagnetic, diamagnetic and unsaturated ferromagnetic (s.l.) contributions to χ_{bulk} are isolated within χ_{hifi} leaving the soft ferrimagnetic contributions to χ_{bulk} isolated within
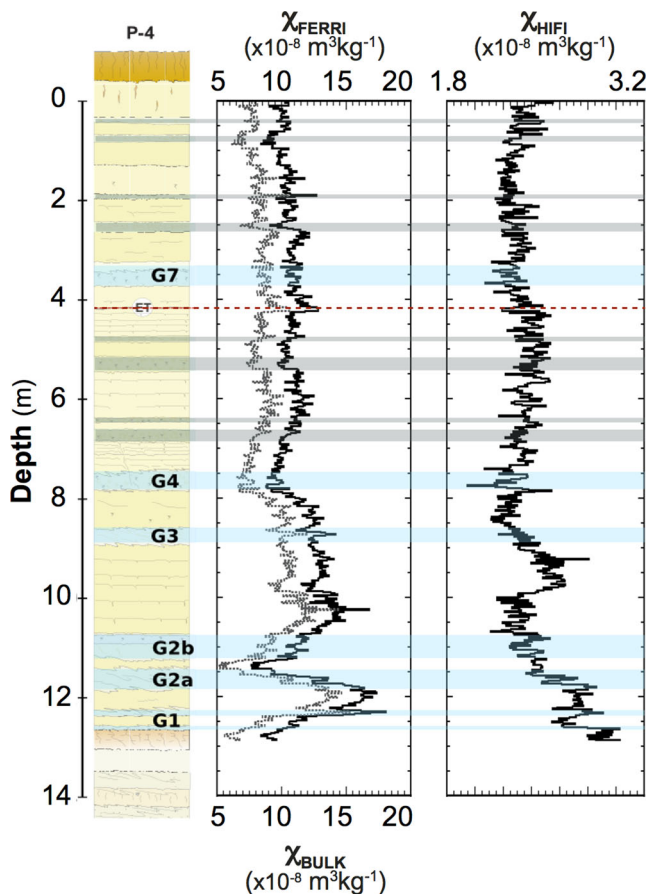
Figure 5. From left to right-hand panel: ferrimagnetic (χ_{ferri}), bulk (χ_{bulk}) and high-field magnetic susceptibility (χ_{hifi}) variations compared to the stratigraphy. The main and incipient tundra gley horizons are highlighted in blue and grey, respectively. The Eltviler Tuff (ET) tephra data at 4.22–4.20 m (red dotted line) are not shown.

Figure 6. Day-Dunlop plot: ratio of saturation remanent magnetization (M_{RS}/M_S) against the ratio of coercivity of remanence to coercive force (B_{CR}/B_C; Day *et al.* 1977). Single domain (SD), pseudo-single domain (PSD) and multidomain (MD) plot boundaries and mixing lines are taken from Dunlop (2002).

χ_{ferri}. It can be concluded that χ_{bulk} variations are dominantly controlled by the soft ferrimagnetic component since χ_{bulk} and χ_{ferri} covary ($R^2 = 0.99$; Figs 5 and 8a). Moreover, χ_{hifi} fluctuates strongly between 13 and 8 m depth either as a result of changes in concentration or mineral composition of the paramagnetic component or the unsaturated (or high coercivity) ferromagnetic (s.l.) component.

Fig. 6 shows that the mean domain state of the mineral magnetic assemblage is pseudo-single domain (PSD) grain size, however given the bias towards magnetite, any inference of grain size has to be taken with caution. Since the data plot to the right of the SD–MD (single domain–multi domain) mixing line (Dunlop 2002) at least one additional magnetic component is likely present.

Fig. 7 shows a selection of hysteresis and remanence parameters correlated to the P4 stratigraphy. Highs of B_C and B_{CR} (mean values in loess of 10.1 ± 1.6 and 39.6 ± 8.3 mT, respectively) correspond to lows in M_S and M_{RS} (means in loess of 10.9 ± 2.4 and 1.2 ± 0.18 mAm^{2}kg^{-1}, respectively). M_S and M_{RS} values covary with χ_{bulk} and χ_{ferri} (Figs 7 and 8b). B_C and B_{CR} have a much 'noisier' signal (Fig. 7), with B_C showing variations of ~5 and ~20 mT, respectively over small depth intervals. Tundra gley horizons generally have higher coercivity values and lower magnetization values than loess, although above ~4 m, B_{CR} in tundra gley horizons (e.g. G7) decreases with respect to surrounding loess (Fig. 7). There is a general increase up profile in the squareness ratio (M_{RS}/M_S) from
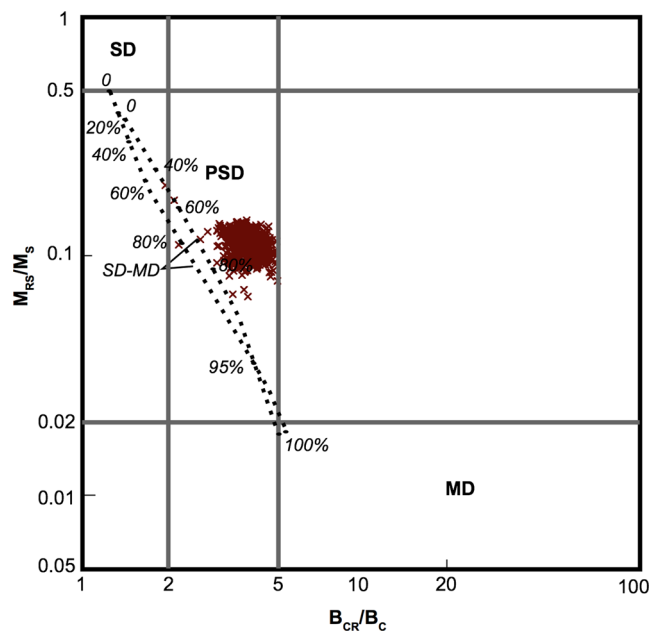
approximately 0.098–0.13, with the largest variations in the lower few metres and a more noticeable jump at ~8 m (Fig. 7).

4.3 IRM experiments

SIRM and M_{RS} covary (Fig. 7) but SIRM intensity is on average 11 per cent (± 6 per cent) weaker than M_{RS} due to the difference in saturating fields, 1T for SIRM and a maximum field of ± 1.5 T for the hysteresis loop from which M_{RS} is determined. This difference foreshadows the influence of high coercivity minerals to the mineral magnetic assemblage along the Nussloch sequence. Low S-ratio values calculated for a backfield of 100 mT (<0.5 for most of the section) indicate that over half of the SIRM$_{(1T)}$ is carried by minerals that have remanent coercivities more than 100 mT. Even with a backfield of 300 mT, the S-ratio average is low at around 0.83 ± 0.03, confirming a significant influence by higher coercivity minerals (e.g. hematite, goethite). The linear correlation between S_{100mT} and S_{300mT} has an R^2 value of 0.78 and 0.54 for the loess and tundra gley sample populations, respectively. Mineralogical changes or relative abundances between high and low coercivity components are relatively constant in the 100–300 mT coercivity of remanence range with respect to the below 100 mT coercivity range for the loess. Variations in SIRM are more closely tracked by S-ratio variations than those observed in HIRM. This is more convincingly observed over the 13–8 m interval where these parameters fluctuate most. HIRM tracks changes in concentration of the high coercivity component. SIRM is dominated by concentration changes in the low coercivity component.

4.4 ARM

ARM variations with depth are subtle in comparison to other parameters (Fig. 7); fluctuating by approximately 0.1×10^{-5} Am^{2}kg^{-1} from a centre of 0.79×10^{-5} Am^{2}kg^{-1}. Even though the two depths
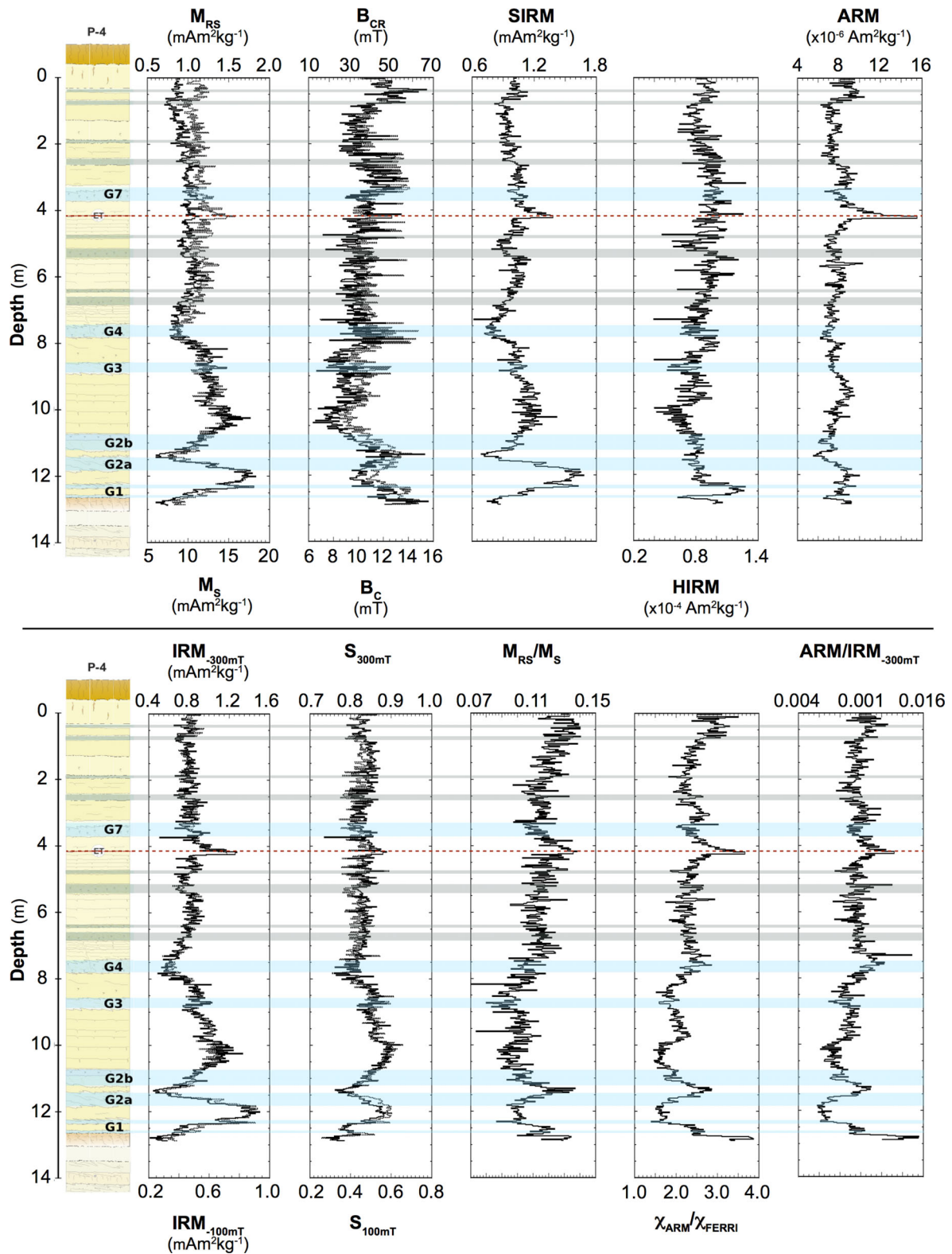
Figure 7. Variations of bulk magnetic parameters and ratios compared to the Nussloch P4 stratigraphy. M_{RS}, B_{CR}, IRM$_{-300mT}$ and S_{300mT} are represented by the dashed lines in their respective plots. Grey and blue shaded horizons represent incipient and main tundra gley units, respectively. The Eltviler Tuff (ET) tephra data at 4.22–4.20 m (red dotted line) are not shown.

dominated by tephra material have been masked, some material may still be present in adjacent layers (Fig. 7). ARM and the bias DC field normalized χ_{ARM} values show no linear correlation with χ_{ferri} (Fig. 8d). This observation is truer for loess ($R^2 = 0.05$) than tundra

gley ($R^2 = 0.24$) intervals. Fig. 8(d) is a plot modified from King *et al.* (1982) where χ is replaced by χ_{ferri} and from which high-sloped trends are defined by finer grained magnetite particles. From Fig. 8(d) it could be argued that loess samples define two trends of
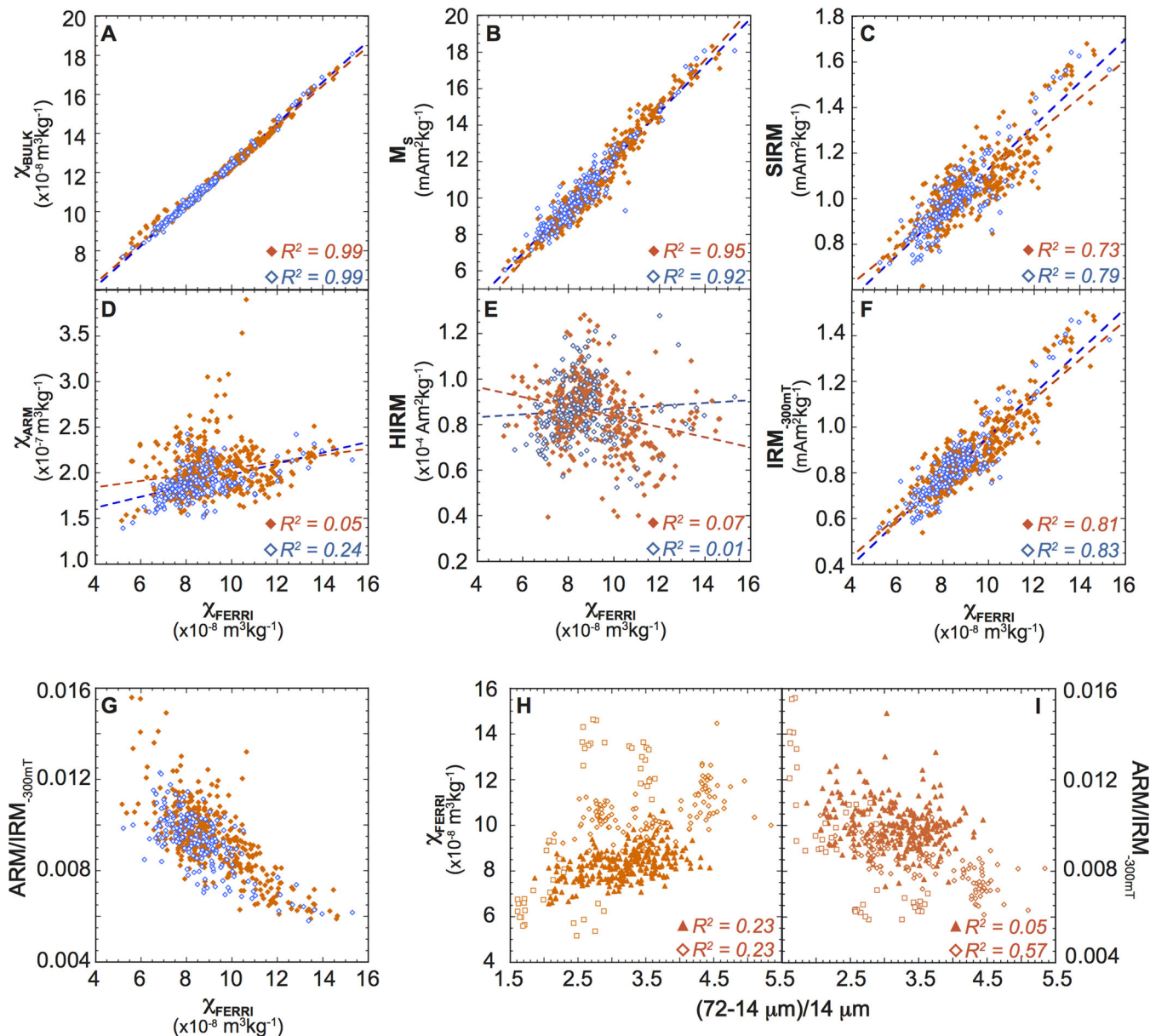
Figure 8. A–G: biplots of ferrimagnetic susceptibility (χ_{ferri}) with various bulk magnetic parameters. Closed orange symbols represent loess sample population and open blue symbols, tundra gley sample population. H–I: biplots of sediment grain size ratio (plotted in Fig. 3) with magnetic concentration (χ_{ferri}) mean ferrimagnetic grain size (ARM/IRM$_{-300mT}$). Open squares = samples from 13 to 11 m, open diamonds = 11–8 m, closed triangles = 8–0 m.

differing slopes leading to the very low correlation coefficient. The higher slope trend is not observed for tundra gley sample population. Fig. 9 highlights a decrease in the absolute values of ARM when moving up profile through underlying loess to a tundra gley horizon.

4.5 Low-temperature experiments

Fig. 10 shows RT-SIRM cooling and warming curves and LT-SIRM ZFC-FC warming curves for selected loess layers (Figs 10a and b) and tundra gley horizons (Figs 10c and d). Normalizing values can be found in Table 1.

For loess samples, upon cooling to around 200 K, there is a 2.5–7.5 per cent increase in remanence from the initial RT-SIRM at 300K. The Verwey transition ($T_V = 115 \pm 15$ K calculated range

from measured samples) is clearly visible (Figs 10a and 11) confirming the presence of magnetite, with each sample showing a 10–25 per cent remanence loss between around 160 and 75 K (through T_V) on cooling (Fig. 10a). The samples at the base of the profile (below 8 m) show the largest remanence loss on cooling through T_V, which indicates coarser-grained magnetite (Özdemir *et al.* 2002). Below 75 K, their remanences remain constant towards 10 K and are reversible upon warming back up to 75 K, with a total remanence loss at 300 K of 15–18 per cent. The loess samples in the upper section of the profile (above 8 m) show an overall increase of remanence on cooling trend, superimposed over the cooling-warming curve behaviour observed in the other samples at the base of the profile. This suggests the presence of maghemite and/or goethite (Rochette & Fillion 1989; Özdemir & Dunlop 2010).
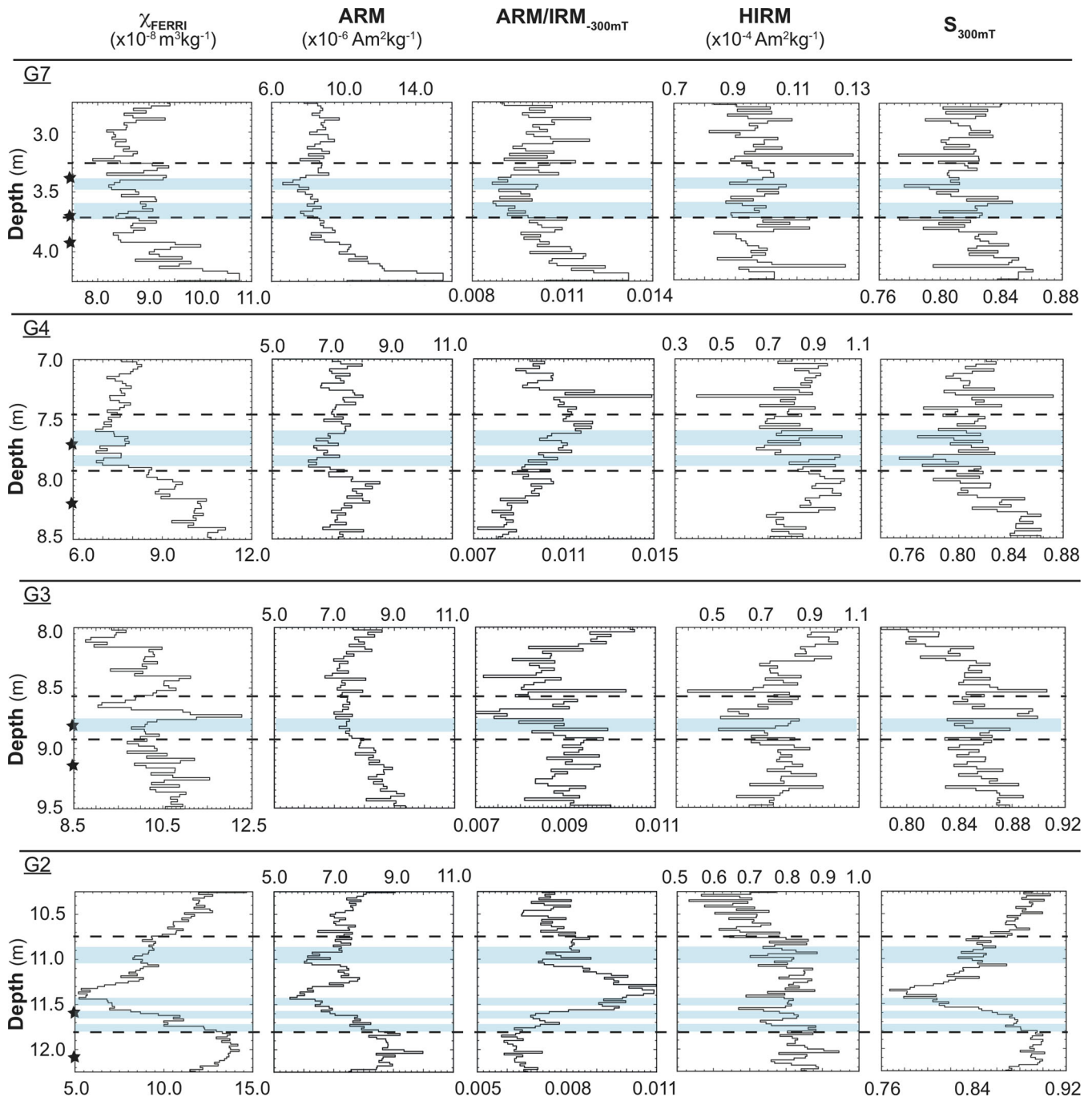
Figure 9. Variations of a selection of magnetic parameters and ratios across the main tundra gley horizons G2, G3, G4 and G7. There upper and lower boundaries as identified in the field (Antoine *et al.* 2009) are marked by dashed lines. Shaded horizons are the intervals over which redoxomorphic processes induced by waterlogging has left an imprint on the magnetic record (see discussion in Section 5.3). Black stars located on the χ_{ferri} figures identify sample depth of low-temperature data shown in Fig. 10.

The initial LT-SIRM at 10 K is at least 50 per cent higher for each loess sample in the FC step than the ZFC step. In warming the samples from 10 K (both for ZFC and FC), each sample shows a general trend of remanence loss and convergence only at 300 K (Fig. 10b). There are marked transitions, highlighted clearer in the ZFC warming curves, at the Verwey transition ($T_V = 110 \pm 10$ K) and also at $\sim$25 K. The loess sample at 12.46 m shows the largest difference in total remanence at 10K between ZFC and FC, with all the deeper samples showing a sharper/steeper T_V.

For tundra gley horizons, the RT-SIRM behaviour with depth is similar to the loess, however samples G2, G4 and IG8b do not show reversible remanence between 10 and 75 K (Fig. 10c). This is likely due to instrument noise. The samples in the lower profile (G1, G2 and G3) show the largest remanence loss through T_V (115 ± 10 K calculated range measured for tundra gley samples) upon cooling. Apart from G1 and G2, all the samples generally show an inclined slope between 10 and 75 K.

As with the LT-SIRM behaviour for the loess, the initial LT-SIRM is at least 50 per cent higher for each tundra gley sample at 10 K for
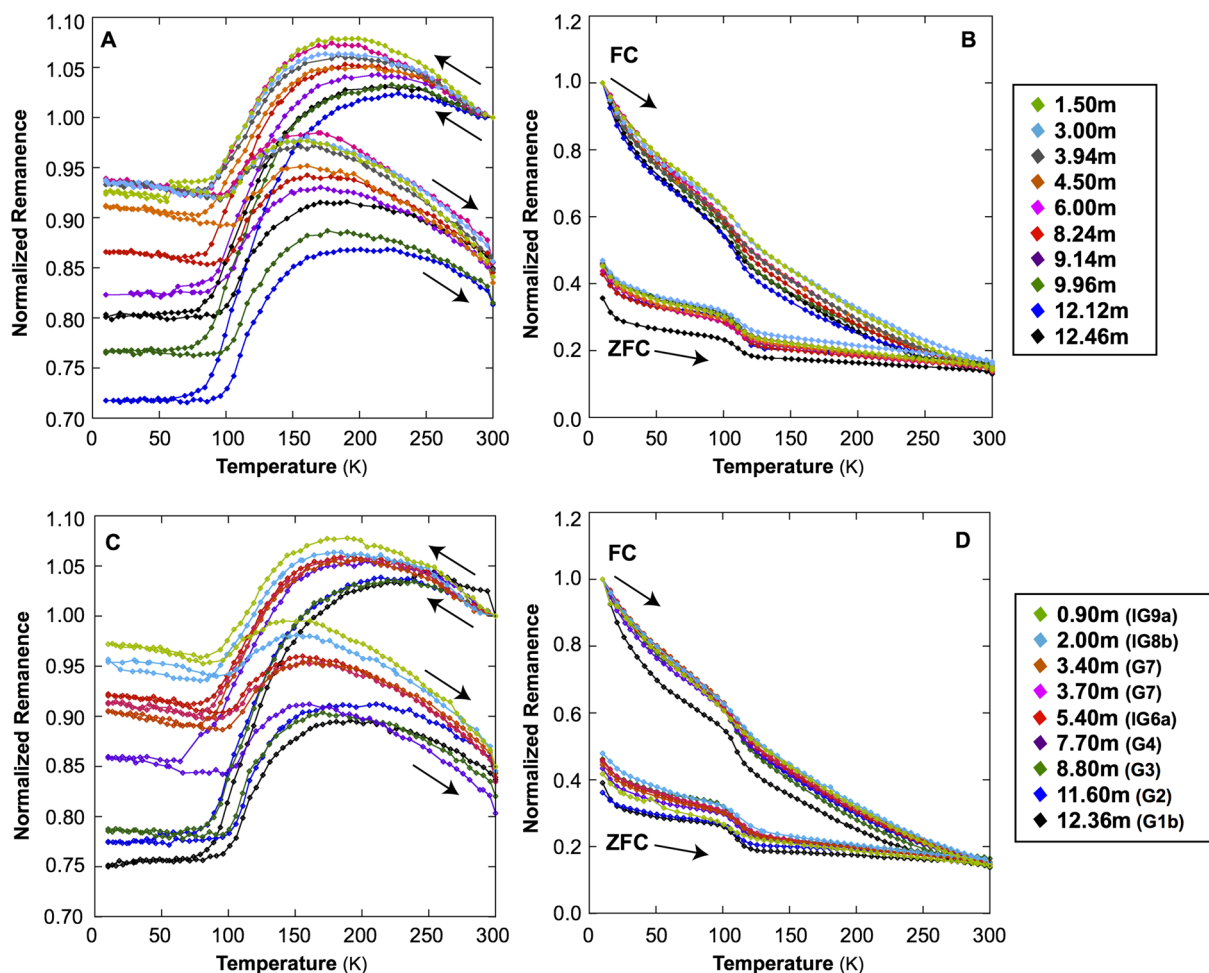
Figure 10. RT-SIRM (a, c) and ZFC/FC (b, d) data for a selection of samples within loess (upper panels) and tundra gley (lower panels) horizons. *Note:* G = main tundra gley; IG = incipient tundra gley. The arrows mark the cooling or warming direction for each curve.

Table 1. Normalizing values for the low-temperature experiments in Fig. 10. Tundra gley samples are denoted with their unit name in parentheses, where G = major tundra gley; IG = incipient tundra gley.

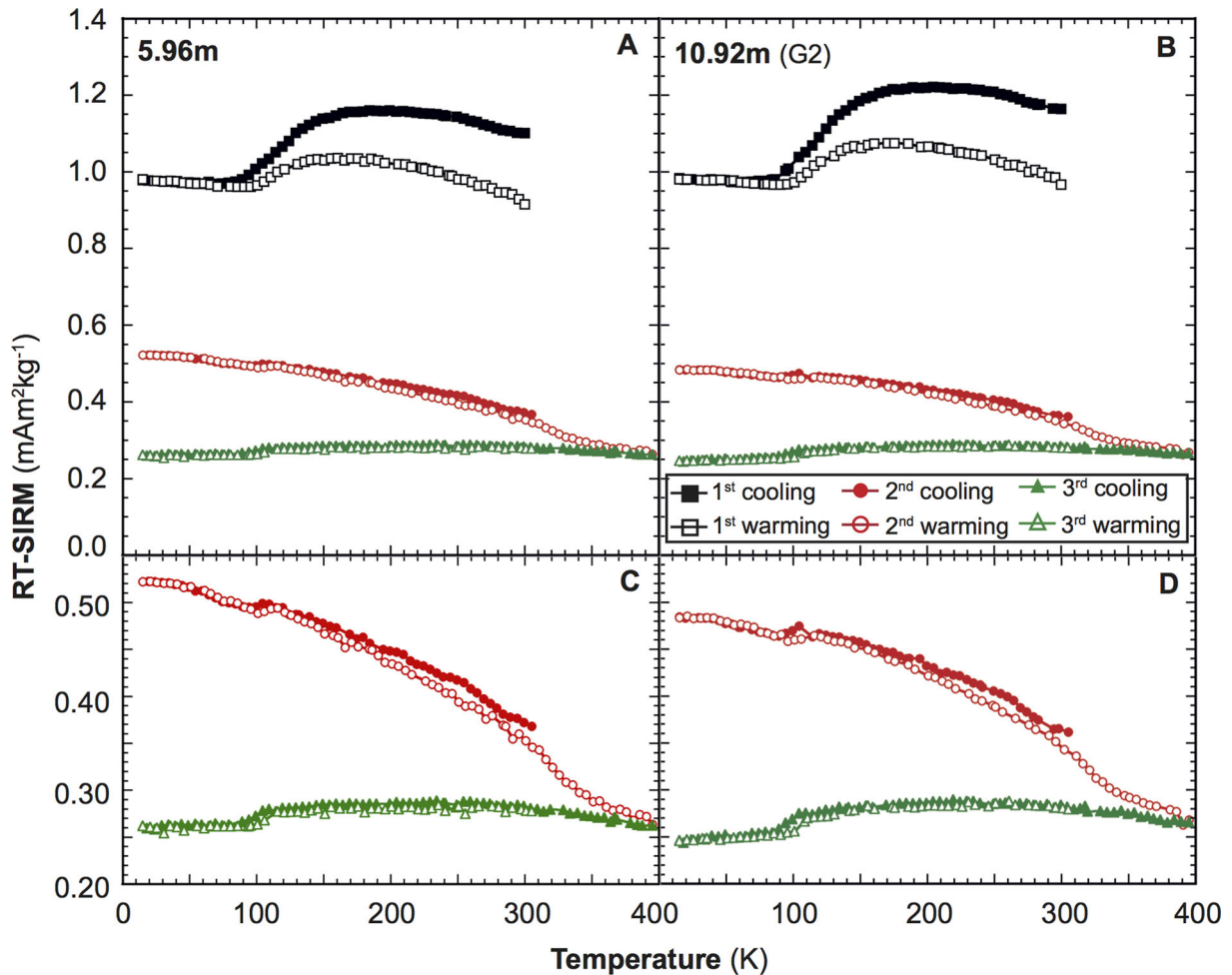| Sample (m)	RT-SIRM at 300 K (mAm^2kg^{-1})	FC LT-SIRM at 10 K (mAm^2kg^{-1})
0.90 (IG9a)	0.9571	0.525
1.50	1.026	0.525
2.00 (IG8b)	1.041	0.518
3.00	1.064	0.500
3.30 (G7)	0.979	0.490
3.70 (G7)	1.074	0.544
3.94	1.226	0.636
4.50	1.133	0.583
5.40 (IG6a)	1.131	0.583
6.00	1.131	0.621
7.70 (G4)	0.940	0.447
8.24	1.042	0.553
8.80 (G3)	1.109	0.4980
9.14	1.187	–
9.96	1.113	0.851
11.60 (G2)	1.175	0.570
12.12	1.491	0.678
12.36 (G1b)	1.410	0.720
12.46	1.209	0.688

Figure 11. Decomposing RT-SIRM following the Guyodo *et al.* (2006) protocol for (A) a loess and (B) a tundra gley specimen. First cycle corresponds to the classic RT-SIRM cooling and warming. The specimen was AF demagnetized with a peak 300 mT field prior to the second cycle. Warming curve of the second cycle continued up to 395 K to thermally demagnetize any goethite present before undergoing the third and final cycle. C and D are zoomed-in for A and B, respectively. See Section 4.5 for information on the experimental procedure and interpretation.

the FC step than the ZFC step (Fig. 10d). Also similar to the deeper loess samples, the lower profile tundra gleys show a sharper and/or larger remanence loss through T_V.

The RT-SIRM was further analysed following the experiment in Guyodo *et al.* (2006), but using a 300 mT AF demagnetization step instead of 200 mT, in order to unravel the magnetic mineral components contributing to the RT-SIRM (Fig. 11). Following the classic RT-SIRM experiment (upper most cycle), an enhanced RT-SIRM was acquired by cooling the sample from 395 to 300 K in a 2.5 T magnetic field and then AF demagnetized in a 300 mT field before cycling to 10 K and back up to 395 K (middle cycle). The AF demagnetization was able to suppress almost all of the magnetite contribution. A small but distinct remanence loss remains near 100 K associated to the Verwey transition of a most likely partially oxidized magnetite component (Özdemir & Dunlop 2010). A significant amount of remanence, attributed to goethite, is demagnetized by heating to 395 K and cooling back to 300 K. In the final cooling and warming (bottom cycle) the increasing remanence with decreasing temperature trend of the middle cycle has also been suppressed confirming that this behaviour is that of goethite. The final cycle does not show any sign of a Morin transition, which we might expect if hematite is present given that both magnetite and goethite behaviours have been suppressed. The Morin transition of

hematite would be observed at 250 K for particle sizes of 100 nm and larger and at progressively lower temperatures for particles sizes less than 100 nm (Fig. 8 in Özdemir *et al.* 2008). This is known from Mössbauer measurements. Temperature dependence behaviour of RT-SIRM or LT-SIRM for fine-grained hematite (<100 nm) is not well documented in the literature. The experiment in Fig. 11 has so far been conducted on a dozen samples, with all showing the same low temperature behaviour.

5 DISCUSSION

5.1 Mineralogy of the magnetic assemblage

The magnetic mineral assemblage and its variability within a loess-palaeosol profile are key for the interpretation of palaeoclimates (Heller & Evans 1995). Due to the high sampling resolution (continuous 2 cm depth interval) of the sequence studied herein, it is possible to see significant small-scale variations that would be missed in lower resolution profiles.

Evidence of magnetite as the main ferrimagnetic mineral is supported by the low-temperature data (e.g. occurrence of the Verwey transition in Figs 10 and 11), but for example, the low *S*-ratio

values also indicate that the mineral magnetic assemblage includes at least one high-coercivity mineral. Given the 1 T maximum field applied to acquire the SIRM and calculate the S-ratios, one may suspect hematite over goethite as the remanence carrier in the 0.3–1 T coercivity window. However, the low temperature magnetism data provide overwhelming evidence for the presence of goethite. The increasing RT-SIRM on decreasing temperature trend observed in Figs 10(a) and (c) and the large gap between FC and ZFC warming remanence curves persisting at temperature greater than 120 K (T_V) in Figs 10(b) and (d) are suggestive of goethite (Banerjee 1970; Rochette & Fillion 1989; Özdemir & Dunlop 1996; Guyodo *et al.* 2006) in both loess and tundra gley samples. The experiments plotted in Fig. 11 and presented in Section 4.5 are conclusive confirming, for both loess and tundra gley sample population, the presence of goethite while providing no evidence for hematite in the low temperature data even after AF demagnetization to 300 mT and thermal demagnetization to 395 K (122 °C). This said the low-temperature remanence behaviour of small (<100 nm) hematite particles is not well documented in the literature. Therefore, we cannot ascertain whether the final RT-SIRM cycling behaviour (green curves in Fig. 11) is characteristic of nanohematite or not. Finally, from these experiments, we observe, after an AF demagnetization in peak field of 300 mT, a Verwey transition, albeit supressed to temperature of 100 K. An incomplete or non-homogeneous oxidation of a magnetite particle has been shown to lead to a higher coercivity of remanence (e.g. van Velzen & Dekkers 1999; Liu *et al.* 2004) and lowering of T_V (Özdemir *et al.* 1993). Therefore, the mineral magnetic assemblage also includes partially oxidized magnetite to maghemite in both loess and tundra gleys. In summary, there appears to be no major differences in mineralogical components between samples within tundra gley horizons, as identified in the field, and the parent loess. The imprint of redoxomorphic processes induced by waterlogged conditions on the mineral magnetic assemblage, if any, will have to be observed in concentration and/or grain size variations which will be discussed in Section 5.4.

5.2 Magnetic characteristics of the parent loess

From the near perfect correlation between χ_{bulk} and χ_{ferri} (Fig. 8a), χ_{ferri} and M_S (Fig. 8b), the very good correlation between ι_{ferri} and SIRM (Fig. 8c) and χ_{ferri} and IRM$_{300mT}$ (Fig. 8f) and the complete absence of correlation between χ_{ferri} and HIRM (Fig. 8e) we can state that the bulk concentration parameters are controlled by soft ferrimagnetic magnetite/maghemite. Moreover, the good correlation between χ_{ferri} and SIRM (Fig. 8c) and the complete absence of correlation between χ_{ferri} and χ_{ARM} (Fig. 8d) suggest a dominant control of the bulk concentration parameters by coarser grained magnetite (MD). This is true because increases in concentration of SD to small PSD magnetite particles will increase ARM values much greater than an equivalent change in MD magnetite concentration. Similarly MD magnetite will impart a greater change in IRM at saturation than the IRM of an SD magnetite grain brought to saturation. The rock magnetic interpretation of concentration changes may be further refined to χ_{bulk}, χ_{ferri}, M_S, SIRM, IRM$_{100mT}$ and IRM$_{300mT}$ tracking changes in coarse MD ferrimagnetic magnetite and maghemite concentrations, to ARM and χ_{arm} tracking changes in SD to small PSD ferrimagnetic magnetite and maghemite concentrations and HIRM tracking high coercivity goethite (and possibly hematite but its presence remains unconfirmed, see Sections 4.5 and 5.1). The primary control on χ variations at Nussloch is therefore coarse-grained magnetite as was previously postulated in Rousseau *et al.* (2002).

The origin of coarse MD magnetite in loess sequences can be no other than detrital in origin and consequently brought to the deposition site via aeolian transport. The same argument does not necessarily hold true for fine-grained SD and PSD magnetite or high coercivity minerals such as goethite and hematite which can be produced *in situ* during pedogenic or diagenetic alterations. The lack of correlation between the concentration parameter for MD magnetite and the concentration parameter for SD to PSD magnetite (Fig. 8d) or goethite (Fig. 8e) suggest that changes in concentration of the latter two components are not dominantly controlled by aeolian transport as MD magnetite concentration changes.

Changes in mean grain size of the ferrimagnetic component may also be tracked via various interparametric ratios. χ_{bulk}/M_S or χ_{ferri}/M_S is most useful to detect SP particles. Given that no SP particles were detected in the loess interval investigated, these parameters are reduced to a concentration only parameter (see Fig. 8b) and are not used for mean magnetic grain size. χ_{arm}/χ_{ferri} or χ_{arm}/χ_{bulk}, when SP particles are absent, can be interpreted as increasing when the mean ferrimagnetic grain size decreases. If a significant amount of high coercivity minerals are present, they will contribute to the denominator and not the numerator resulting in a bias of these proxies to coarser mean grain size. Given the low S_{-100mT} and S_{-300mT} (Fig. 7) χ_{arm}/χ_{ferri} would be preferred for the Nussloch loess sequence, but a pollution of χ_{ferri} by a significant high coercivity component remains possible given that the hysteresis high field slope correction was performed over the 1–1.5 T branch segment and particles saturating up to 1 T will be included in the calculated χ_{ferri}. This can be circumvented by using ARM/IRM$_{100mT}$ or ARM/IRM$_{300mT}$ as a mean ferrimagnetic grain size proxy. The latter is also circumstantial but Fig. 7 shows the high level of coherence between IRM$_{100mT}$ and IRM$_{300mT}$ which is confirmed by an R^2 positive linear correlation coefficient of 0.92 and 0.88 for the loess and tundra gley sample population respectively (not shown). Any pollution of IRM$_{300mT}$ by high coercivity, non-ferrimagnetic minerals should be very minor. The bulk of the IRM acquired between 100 and 300 mT is likely from partially oxidized magnetite as suggested by the low temperature experiment in Fig. 11 (see also Section 4.5). Fig. 7 shows that χ_{arm}/χ_{ferri} and ARM/IRM$_{300mT}$ covary significantly. They show a positive linear correlation with an R^2 coefficient of 0.80 and 0.70 in loess and tundra gley sample population, respectively (not shown) and therefore can be used interchangeably as a mean ferrimagnetic grain size proxy. The most obvious divergence between these proxies is observed immediately below G3 tundra gley over the ~10 and 9 m interval where χ_{arm}/χ_{ferri} displays increasing mean ferrimagnetic grain size and ARM/IRM$_{300mT}$ decreasing mean ferrimagnetic grain size. Coincidentally, a jump to higher HIRM values is observed going into this interval (Fig. 7). As stated above a significant high coercivity component would bias χ_{arm}/χ_{ferri} to coarser ferrimagnetic grain size.

The wind vigour model for loess magnetism expects both concentration and mean magnetic grain size to increase with increasing wind speed (Béget *et al.* 1990; Evans 2001). Events of higher wind speeds are expected to be more frequent during glacial periods than interglacial periods and similarly more frequent during glacial stadials than glacial interstadials. We observe in loess intervals increasing MD ferrimagnetic particle concentration (χ_{ferri}) with increasing mean ferrimagnetic grains size (ARM/IRM$_{300mT}$) in agreement with the wind vigour model (Fig. 8). Sedimentological grain size of the studied interval, shown in Figs 3 and 12, was proposed in Antoine *et al.* (2009) to show coarsening grain size distributions penecontemporaneously with Heinrich stadials and similarly fining grain size distributions associated with tundra gley units formed
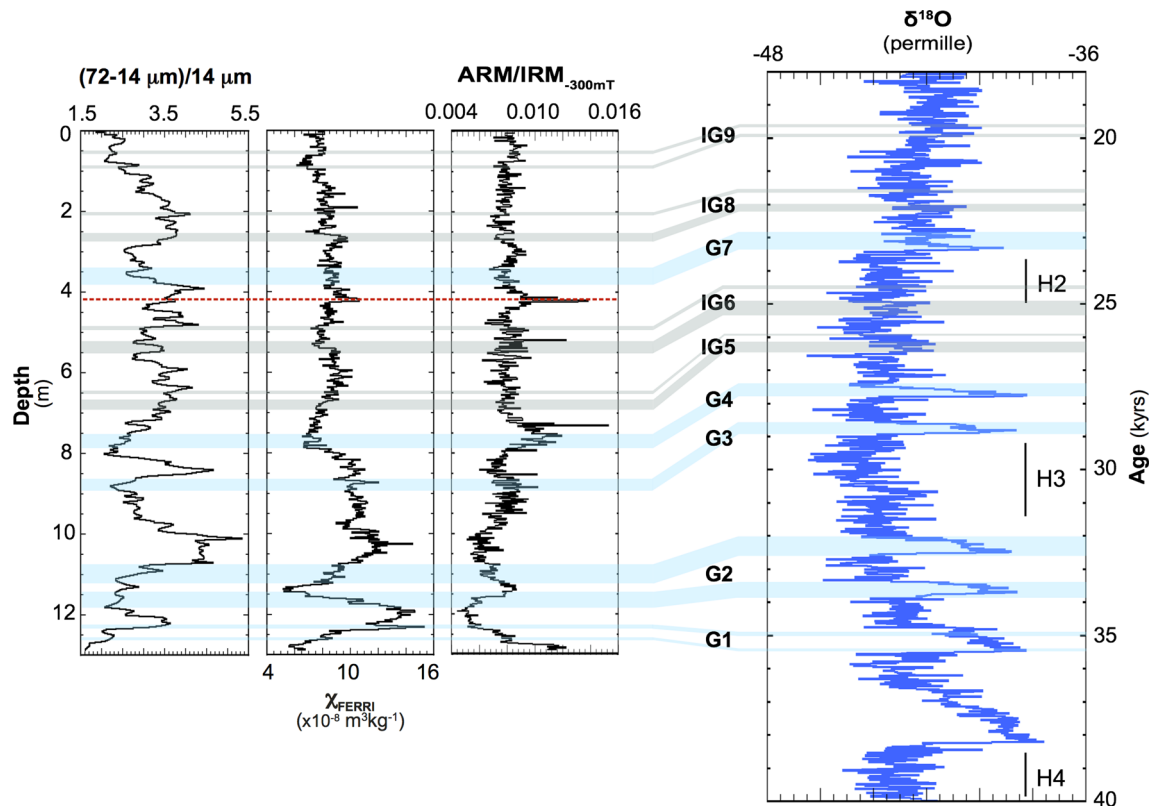
Figure 12. Comparison between ferrimagnetic susceptibility (χ_{ferri}), grain size data (Antoine *et al.* 2009), mean ferrimagnetic grain size (ARM/IRM$_{-300\text{mT}}$) and variations in the oxygen isotope record in the Greenland ice at NGRIP (NGRIP 2004). The tie lines are based on previous work done by Rousseau *et al.* (2007) and Antoine *et al.* (2009), where pale blue lines represent the major tundra gley horizons (G), grey for incipient tundra gleys (IG) and the dotted red line for the Eltviller tephra layer (ET). The tie lines for the incipient tundra gleys were subjectively included and therefore an associated specific warming event must be taken with caution. H = approximate position of Heinrich Stadials (based on Bond *et al.* 1993; Hemming 2004).

during D-O interstadials. There are no to very little physical grain size overlap between magnetic grain size proxies and measured sedimentological grain size distributions. The clay to silt grain size limit is routinely set at ~4 μm, a grain size for which magnetically magnetite is well into the MD range. Therefore perfect correlation between magnetic grain size proxies, which by their definition vary dominantly as a function of changes in magnetite concentration of SP (<0.03 μm), SD (0.03–0.1 μm) or small PSD (0.1 to ~1 μm) particles and sedimentological grain size should not be expected. Moreover, as the ferrimagnetic grain size becomes dominated by MD particles, magnetic grain size proxies appear to become invariant with increasing concentration (Fig. 8g). Therefore while MD ferrimagnetic concentration parameters should not saturate at its upper limit, we should expect ferrimagnetic grain size proxies to saturate at the coarsest grain size limit.

The two independent wind vigour proxies considered for the studied loess interval are compared in Figs 8(h), (i) and 12. The stratigraphic correlation between these proxies as illustrated in Fig. 12 is difficult to visually evaluate because the amplitude of variations are much greater for the coarse silt index then either of the magnetism based proxies for wind strength. This is especially true for the upper unit spanning the 8–0 m depth interval. The biplots of Figs 8(h) and (i) facilitate this evaluation and a certain amount of stratigraphic interpretation is achieved by plotting separately the three main units presented in Section 2 and discussed in Section 5.3. In general, the coarse silt index against χ_{ferri} (magnetic concentration) and ARM/IRM$_{-300\text{mT}}$ (mean ferrimagnetic grain size)

show that the sedimentary grain size increases with both increasing magnetic concentration and increasing mean ferrimagnetic grain size. However, certain intervals do not convincingly follow this trend and define instead distinct clusters. The lower unit (13–11 m) displays the highest amplitude variations in concentration of high coercivity minerals as exemplified in HIRM (Fig. 7) and χ_{hifi} (Fig. 5) and therefore χ_{ferri} is not isolating as efficiently the concentration of MD ferrimagnetic particles (wind strength proxy) leading to the poor correlation in comparison to the two upper units. The mean magnetic grain size proxy for wind strength correlates best with the coarse silt index for unit 2 (11–8 m) with an R^2 value of 0.57 (Fig. 8i).

In summary, variations in concentration of coarse MD ferrimagnetic particles is shown to dominate the fluctuations observed in bulk concentration parameters χ_{bulk}, χ_{ferri}, M_S and SIRM and not the concentration of SD to small PSD ferrimagnetic particle nor that of high coercivity minerals. The origin of MD ferrimagnetic particles can only be of detrital origin and consequently of aeolian deposition. Any post-depositional remobilization, the only alternative to wind deposition for the occurrence of MD ferrimagnetic particles, is currently being evaluated through a magnetic anisotropy study. Assuming that the coarse silt index is an accurate proxy for wind strength, χ_{ferri} and/or ARM/IRM$_{-300\text{mT}}$ can proxy for wind strength in Upper Pleniglacial Nussloch loess, outside of the 13–11 m interval, following the wind-vigour model as previously done in Alaska (Béget *et al.* 1990; Lagroix & Banerjee 2004b) and Siberia (Chlachula *et al.* 1997; Matasova *et al.* 2001).

5.3 Magnetic characteristics of tundra gley horizons

While the mineralogical assemblage of the tundra gley horizon is unchanged from that of the parent loess material, the concentration and grain size magnetic parameters at Nussloch appear to indicate that tundra gleys have been altered with respect to the parent loess.

The imprint of diagenetic alteration within the tundra gley horizons on the mineral magnetic record is evaluated with respect to an initial state constrained by the following. First, the stratigraphic boundaries of the tundra gleys are based on field observations of discolouration (see Section 2). Their upper and lower boundaries are drawn as dashed lines in Fig. 9. Second, given that tundra gley horizons along P4 are underlined by higher TOC and weak decalcification and carbonate precipitation, there is evidence for soil formation (Antoine *et al.* 2009; Gocke *et al.* 2013) and consequently climate amelioration. As mentioned previously, the wind vigour model postulates that wind strength (and therefore grain size of deposited dust) decreases with climate amelioration (Evans 2001). Therefore a decrease in the primary loess magnetic mineral concentration and grain size is expected to be associated with the tundra gley horizon identified in the field. Any imprint of diagenetic alteration on the magnetic record will be superimposed onto this initial state and may or may not imprint or overprint the entire tundra gley interval defined by field observations.

The large-scale variations of coarse-grained ferrimagnetic concentration parameters (χ_{ferri}) define a broad minimum in which the main tundra gley horizons G2, G4 and G7 are included and less convincingly for G3 (Fig. 9). The broad local minimum observed in all four main tundra gleys for ARM, which is strictly a ferrimagnetic concentration parameter but more influence by changes in SD to small PSD particles than MD, is much better defined. Considering the total tundra gley sample population, decreasing ferrimagnetic concentration is accompanied by a fining of the mean ferrimagnetic grain size (Fig. 8g) agreeing with the wind vigour model. However stratigraphically, this trend is only convincingly observed (Fig. 9), at a large scale, through G2 and G4. The large-scale trend through G7 defines a broad coarsening of ferrimagnetic mean grain size with decreasing magnetic concentration, in complete opposition to the wind vigour model. This apparent contradiction suggests that the correlation observed at the tundra gley sample population scale (Fig. 8g) must be stratigraphically expressed over shorter depth scales.

Nawrocki *et al.* (1996) found magnetic depletion in gleyed and leached horizons in Polish and Ukrainian loess-palaeosol sequences. A similar interpretation was introduced for nearby sites in SW Germany of hydromorphic conditions causing the decomposition of iron under reduced conditions (Terhorst *et al.* 2001). For loess-palaeosol deposits in Saxony, layers influenced by periodical waterlogging (solifluction layers and gleyed palaeosols) show a noticeably large drop in magnetic susceptibility (Baumgart *et al.* 2013). It is postulated that fine-grained magnetite/maghemite minerals are preferentially dissolved under water-saturated, reducing zones over coarser particles, leading to a coarser-grained magnetic mineral signature in parts of the altered horizons. Thereafter, liberated ferrous iron is available to reprecipitate once dry oxidizing conditions return, and as a result increasing the magnetic hardness of altered horizons (Xu *et al.* 1997; Rowan *et al.* 2009). During warmer or more humid periods, frozen ground (permafrost) prevents water from percolating downwards (Frechen *et al.* 2003; Kimble 2004). At these boundaries water may stagnate leading to anoxic conditions and dissolution of pre-existing iron oxides. Soluble Fe^{2+} upon the return of oxic conditions, would be available for *in situ* mineraliza-

tion of new iron oxides favouring Fe^{3+} oxides and oxyhydroxides (Liu *et al.* 1999).

The weak dissolution and reprecipitation of carbonates found in the tundra gleys at Nussloch (Antoine *et al.* 2001, 2009) could be a result of waterlogging. The shaded depth interval in Fig. 9 all show decreasing ferrimagnetic concentration more clearly in ARM than in χ_{ferri} (see explanation below). In contradiction with the wind-vigour model, these intervals have coarser mean ferrimagnetic grain sizes with respect to the immediately adjacent depth intervals above and below. Dissolution due to waterlogging would preferentially dissolve SD and small PSD particles before dissolving MD particles resulting in a decrease in magnetic concentration and an increase in mean magnetic grain size, as is observed in the shaded depth intervals of Fig. 9. Therefore, it is concluded that the shaded depth intervals have isolated the discrete depth interval having experienced water saturation leading to the dissolution of fine grain ferrimagnetic particles.

The lower three shaded intervals of G2 do not show clear minimums in χ_{ferri} but do show clear maximums in HIRM with respect to the immediately adjacent unshaded depth intervals. As explained in Section 5.2, χ_{ferri} will incorporate high coercivity minerals whose IRM is saturated below 1T. Therefore over depth intervals where HIRM is relatively high and where the proportion of low to high coercivity contributions to SIRM varies significantly, as is the case here based on S_{300mT}, the small-scale variations in χ_{ferri} will be more complex to interpret. These local maximums in HIRM are seen within every shaded horizon in Fig. 9, with the exception of those in G7 (discussed below) but only in the above example are they associated with rapid changes in S_{300mT}. In Sections 4.5 and 5.1 we argued for goethite as the dominant high coercivity mineral. Hematite is not excluded but there is no categorical evidence of its presence and moreover there is an obvious need to better understand and characterize the low temperature magnetic behaviour of small (<0.1 µm) hematite particles. The environmental conditions leading to the dissolution of the fine ferrimagnetic particles would have had the same effect on goethite, if present initially. The mineralogical data presented in Section 5.1 heavily suggest that goethite was in part deposited with the primary loess, possibly as coatings on quartz grain as is often observed (e.g. Penn *et al.* 2001). The HIRM maximums in the shaded depth intervals are in all likelihood due, in part, to *in situ* mineralization during the later stages of redoxomorphic processes under dry oxidizing conditions. Interestingly, the incipient tundra gleys behave similarly to the main tundra gleys with respect to imprints of dissolution on the magnetic record (shaded horizons in Fig. S1), but none of them including main tundra gley G7 display clear maximums in HIRM with respect to the immediately adjacent depth intervals. The climate was increasingly colder up profile; the favourable conditions for waterlogging-induced redoximorphic processes (i.e. increased humidity, subsidence of the active layer) likely persisted over increasingly shorter time periods. This observation of a drier climate up-section has been previously indicated from a change in mollusc species (Moine *et al.* 2005) and $\delta^{13}C$ data (Hatté *et al.* 1999; Hatté & Guiot 2005) at Nussloch and from rock magnetic arguments in Saxonian loess (Baumgart *et al.* 2013). The absent or negligible *in situ* neoformation of high coercivity minerals in tundra gley intervals of G7 and of all incipient tundra gleys (shaded horizons in Fig. 9) despite the observed dissolution of fine grained ferrimagnetic particles suggests that a return to dry oxic conditions is inhibited when favourable conditions for tundra gley formation are time limited.

Maher (2011) discussed the importance in understanding goethite/hematite in tracing aeolian fluxes through space and time. The results herein show that with some additional experimental efforts, it may be possible to quantify the (relative) concentration of detrital versus environmentally controlled *in situ* mineralized antiferromagnetic minerals bettering semi-quantitave models of palaeoprecipitation and/or palaeotemperature. Orgeira *et al.* (2011) developed a model describing magnetic enhancement in soils due to pedogenic magnetite formation based on a statistical treatment of the soil–water balance. Including the production rate of, for example, hematite and goethite into the Orgeira *et al.* (2011) 'magnetic enhancement proxy (MEP)' may result in more accurate palaeo-rainfall estimates where pedogenic ultrafine magnetite particles are not observed.

As a final remark, the magnetic signature of diagenetic alteration within tundra gley horizons does not support an early stage soil development process. According to the pedogenic enhancement model (Zhou *et al.* 1990; Maher & Thompson 1991), the *in situ* formation of fine-grained magnetite/maghemite particles is associated with increased magnetic susceptibility within palaeosol horizons (see for example, Dearing *et al.* 1997; Geiss *et al.* 2008; Orgeira *et al.* 2011). No magnetic enhancement or *in situ* mineralization of SP or SD particles is observed within tundra gley horizons with one notable exception in G2. Here, superimposed on the broad scale decrease in ferrimagnetic concentration, the 11.30–11.00 m interval displays a local maximum in ferrimagnetic concentration associated with a decrease in mean ferrimagnetic grain size. This is in contradiction with the wind vigour loess magnetism behaviour but compatible with a pedogenic enhancement model minus the presence of SP behaviour. The observations presented in this study clearly demonstrate that redoxomorphic processes induced by waterlogging processes have dissolved fine-grained SD to PSD ferrimagnetic particles in discrete horizons within the field identified tundra gleys horizons. At their base, where non-magnetic evidence for pedogenesis is reported (Antoine *et al.* 2009; Gocke *et al.* 2013) behaviour associated with pedogenic magnetic enhancement (increased ferrimagnetic concentration and increase in fine SP and SD particles) are not observed. Gocke *et al.* (2014) equally did not observe any magnetic enhancement in the tundra gley horizons. In lieu of such evidence, this environmental magnetism study does not account for any pedogenic processes during the Upper Pleniglacial loess along the P4 section at Nussloch.

5.4 Environmental evolution

Based on the interpretations argued in Sections 5.1–5.3, the magnetic record, along with previously published data, account for an environmental evolution through time at Nussloch. This evolution is presented below and chronologically constrained by the age model presented in Antoine *et al.* (2009).

(1) ~37 to ~32 kyr (~13–11 m). A wide range of magnetic properties, displaying large-amplitude fluctuations (Fig. 7). The concentration of ferrimagnetic minerals (χ_{ferri}), shown to be dominated by MD particles, increases with increasing mean ferrimagnetic grain size (ARM/IRM-$_{300mT}$; Figs 7, 8g, and 12) throughout this interval suggesting the variations are linked to the wind-blown parent material. However, their use as a wind strength proxy in this interval is tenuous; multiple sediment sources as suggested by Rousseau *et al.* (2002) may be at the origin of the difficult reading as suggested by the clustering of populations and highly variable mean ferrimagnetic grain size over this 2 m loess interval (Figs 8h and i).

Rapidly changing environmental conditions are also to be considered given the number of tundra gley horizons observed (i.e. D-O events) within the short depth range and the relatively low sedimentation rate compared to the next period. Magnetically, the two main tundra gley units (G1, G2) mark a decrease in the concentration of soft magnetic minerals and coarsening of the magnetite grain size (χ_{ferri} and ARM/IRM$_{300mT}$, respectively in Fig. 9), which was further interpreted in Section 5.3.

(2) ~32 to ~27 kyr (~11–8 m). Marked by a stable, relative high in the proportion of soft magnetic minerals (higher *S*-ratio and lower HIRM/SIRM) and coarsening of the magnetite magnetic domain size (as observed by relatively low values of M_{RS}/M_S and ARM/IRM$_{300mT}$) (Fig. 7). By considering the correlation with previous sediment grain size variations, it has been suggested that the increase in susceptibility is due to a detrital input of coarse silt size and magnetically richer material (Antoine *et al.* 2009) and is supported by evidence provided herein (Figs 8h and i). ARM/IRM$_{300mT}$ values decreasing with increasing ferrimagnetic grain size (Fig. 7) are concomitant with increases in coarse-silt (Fig. 8i). This period of time is synchronous with Heinrich stadial 3 (Fig. 12), of which cool and dry climates are expected (e.g. Sima *et al.* 2009, 2013). It is proposed that in the input of coarser-grained ferrimagnetic and paramagnetic material, as observed through χ_{hifi} (Fig. 5), results from episodes of strong winds and/or exposure of a new local source. This local source candidate could be dried, braided river sediments from the Rhine Valley as originally proposed by Antoine *et al.* (2001, 2009) and Rousseau *et al.* (2002).

(3) ~27 to ~18 kyr (~8–0 m). Each magnetic parameter is fairly homogeneous, with no large-amplitude fluctuations (Fig. 7, excluding the tephra). Here, there is a relative low in the proportion of soft magnetic minerals, while simultaneously the ferrimagnetic mean magnetic grain size has also decreased (Fig. 7). The relative lack of variation in magnetic parameters suggests no major changes of provenance of the input material and/or post-depositional alteration; that is, a period where climate and the local environment were in a steadier state. By comparing to NGRIP oxygen isotope records (Fig. 12), this is a period characterized by only one D-O event at around 23 kyr as depicted by tundra gley G7 (also corresponding to Heinrich stadial 2; NGRIP 2004).

6 CONCLUSION

Detailed rock-magnetic measurements of the 2 cm resolution sampling of the Nussloch P4 Upper Pleniglacial loess profile has resulted in the following conclusions:

(1) The magnetic mineral assemblage is composed of magnetite, partially oxidized magnetite (maghemite) and goethite. Signature behaviour of hematite, such as the Morin transition was not observed, but the occurrence of hematite is not excluded, however if present, its concentration is much inferior to that of goethite. The same magnetic mineral assemblage is observed in loess and tundra gley sample populations providing evidence that all of the above minerals have at the very least a detrital aeolian origin.

(2) Variations in concentration of coarse MD ferrimagnetic particles is shown to dominate the fluctuations observed in bulk concentration parameters χ_{bulk}, χ_{ferri}, M_S and SIRM and not the concentration of SD to small PSD ferrimagnetic particle nor that of high coercivity minerals. The origin of MD ferrimagnetic particles can only be of detrital origin and consequently of aeolian deposition. Of these bulk concentration parameters χ_{ferri} is the least susceptible to being polluted by the significant high coercivity component

and provides the best wind strength magnetism based proxy for the Upper Pleniglacial loess at Nussloch.

(3) A secondary control on the magnetic record is associated with waterlogging-induced redoxomorphic processes. Discrete depth intervals, within the tundra gley horizons, display decreasing ferrimagnetic concentration and increasing mean ferrimagnetic grain size which contradicts the wind vigour model for loess magnetism and provides evidence for dissolution of fine grained ferrimagnetic particles as a consequence of waterlogging during wetter/warmer periods.

(4) Intervals showing dissolution within main tundra gley G2, G3 and G4 underwent a subsequent phase of goethite (hematite ?) *in situ* mineralization under renewed oxic conditions.

(5) Redoxomorphic processes can lead to misinterpretation of magnetic susceptibility variations following the wind vigour or pedogenic enhancement magnetism models. By decomposing the magnetic signal with targeted rock magnetic parameters and low temperature magnetism the impact of these processes may be assessed and a correct interpretation may be reached.

(6) Through the Weichselian Upper Pleniglacial, the environment evolves from a warmer, humid climate towards a relatively drier, cooler climate, where the detrital input of minerals is steadier and post-depositional alteration is less prominent. Conditions favourable for tundra gley formation persist over increasingly shorter periods of time as we move up section through the P4 Upper Pleniglacial loess deposit. Major tundra gley horizons become sparser and the characteristic goethite (hematite ?) *in situ* mineralization signature observed in older tundra gleys is absent for the youngest tundra gleys, G7 and incipient tundra gleys found in the uppermost section.

REFERENCES

Antoine, P., Rousseau, D.D., Lautridou, J.P. & Hatté, C., 1999. Last interglacial-glacial climatic cycle in loess-palaeosol sucessions of north-western France, *Boreas,* **28**(4), 551–563.

Antoine, P., Rousseau, D.D., Zöller, L., Lang, A., Munaut, A.V., Hatté, C. & Fontunge, M., 2001. High-resolution record of the last Interglacial-glacial cycle in the Nussloch loess-palaeosol sequences, Upper Rhine Area, Germany, *Quarter. Int.,* **76/77**, 922–112.

Antoine, P., Rousseau, D.D., Hatté, C., Zöller, L., Lang, A., Fontunge, M. & Moine, O., 2002. Événements éoliens rapides en contexte loessique: l'exemple de la séquence du Pléniglaciaire supérieur weichselien de Nussloch (Vallée du Rhin-Allemagne), *Quaternaire,* **13**(3–4), 199–208.

Antoine, P., Rousseau, D.D., Moine, O., Kunesch, S., Hatté, C., Lang, A., Tissoux, H. & Zöller, L., 2009. Rapid and cyclic aeolian deposition during the Last Glacial in European loess: a high-resolution record from Nussloch, Germany, *Quarter. Sci. Rev.,* **28**, 2955–2973.

Banerjee, S.K., 1970. Origin of thermoremanence in goethite, *Earth planet Sci. Lett.,* **223**, 335–348.

Baumgart, P., Hambach, U., Meszner, S. & Faust, D., 2013. An environmental magnetic fingerprint of periglacial loess: records of Late Pleistocene loess-palaeosol sequences from Eastern Germany, *Quarter. Int.,* **296**, 82–93.

Begét, J.E., Stone, B.D. & Hawkins, D.B., 1990. Paleoclimatic forcing of magnetic susceptibility variations in Alaskan loess during the late Quaternary, *Geology,* **18.1**, 40–43.

Bibus, E., Frechen, M., Kösel, M. & Rähle, W., 2007. Das jungpleistozäne Lößprofil von Nußloch (SW-Wand) im Aufschluss der Heidelberger Zement AG, *Eiszeitalter und Gegenwart,* **56**(4), 227–255.

Bond, G., Broecker, W., Johnsen, S., McManus, J., Labeyrie, L., Jouzel, J. & Bonani, G., 1993. Correlations between climate records from North Atlantic sediments and Greenland ice, *Nature,* **365**(6442), 143–147.

Bond, G. *et al.*, 1997. A Pervasive millennial-scale cycle in North Atlantic Holocene and glacial climates, *Science,* **278**(5341), 1257–1266.

Buggle, B., Hambach, U., Müller, K., Zöller, L., Marković, S.B. & Glaser, B., 2014. Iron mineralogical proxies and Quaternary climate change in SE-European loess-paleosol sequences, *Catena,* **117**, 4–22.

Chlachula, J., Evans, M.E. & Rutter, N.W., 1997. A magnetic investigation of a late Quaternary loess/palaeosol record in Siberia, *Geophys. J. Int.,* **132**, 128–132.

Dansgaard, W. *et al.*, 1993. Evidence for general instability of past climate from a 250-kyr ice-core record, *Nature,* **364**(6434), 218–220.

Day, R., Fuller, M. & Schmidt, V.A., 1977. Hysteresis properties of titano-magnetites: grain-size and compositional dependence, *Phys. Earth planet. Inter.,* **13**(4), 260–267.

Dearing, J.A., Bird, P.M., Dann, R.J.L. & Benjamin, S.F., 1997. Secondary ferrimagnetic minerals in Welsh soils: a comparison of mineral magnetic detection methods and implications for mineral formation, *Geophys. J. Int.,* **130**(3), 727–736.

Derbyshire, E., 2001. Characteristics, stratigraphy and chronology of loess and palaeosols, and their application to climatic reconstruction: a preface, *Quarter. Int.,* **76/77,** 1–5.

Dunlop, D.J., 2002. Theory and application of the Day plot (Mrs/Ms versus Hcr/Hc) 1. Theoretical curves and tests using titanomagnetite data, *J. geophys. Res.,* **107**(B3), 2056.

Evans, M.E., 2001. Magnetoclimatology of aeolian sediments, *Geophys. J. Int.,* **144**(2), 495–497.

Evans, M.E. & Heller, F., 2001. Magnetism of loess/palaeosol sequences: recent developments, *Earth-Sci. Rev.,* **54**(1), 129–144.

Evans, M.E. & Heller, F., 2003. *Environmental Magnetism: Principles and Applications of Enviromagnetics,* Vol. 86, International Geophysics Series, Elsevier Academic Press.

Frechen, M., Oches, E.A. & Kohfeld, K.E., 2003. Loess in Europe—mass accumulation rates during the last glacial period, *Quarter. Sci. Rev.,* **22**(18), 1835–1857.

Geiss, C.E. & Zanner, C.W., 2007. Sediment magnetic signature of climate in modern loessic soils from the Great Plains, *Quarter. Int.,* **162–163**, 97–110.

Geiss, C.E., Egli, R. & Zanner, C.W., 2008. Direct estimates of pedogenic magnetite as a tool to reconstruct past climates from buried soils, *J. geophys. Res.,* **113**, B11102, doi:10.1029/2008JB005669.

Gendler, T.S., Heller, F., Tsatskin, A., Spassov, S., Du Pasquier, J. & Faustov, S.S., 2006. Roxolany and Novaya Etuliya key sections in the western Black Sea loess area: Magnetostratigraphy, rock magnetism and paleopedology, *Quarter. Int.,* **152**, 78–93.

Gocke, M., Gulyás, S., Hambach, U., Jovanović, M., Kovács, G., Marković, S.B. & Wiesenberg, G.L., 2013. Biopores and root features as new tools for improving paleoecological understanding of terrestrial sediment-paleosol sequences, *Palaeogeogr., Palaeoclimatol., Palaeoecol.,* **394**, 42–58.

Gocke, M., Hambach, U., Eckmeier, E., Schwark, L., Zöller, L., Fuchs, M., Löscher, M. & Wiesenberg, G.L.B., 2014. Introducing an improved multi-proxy approach for paleoenvironmental reconstruction of loess-paleosol archives applied on the Late Pleistocene Nussloch sequence (SW Germany), *Palaeogeogr., Palaeoclimatol., Palaeoecol.,* **410**, 300–315.

Guyodo, Y., LaPara, T.M., Anschutz, A.J., Penn, R.L., Banerjee, S.K., Geiss, C.E. & Zanner, W., 2006. Rock magnetic, chemical and bacterial community analysis of a modern soil from Nebraska, *Earth planet. Sci. Lett.,* **251**(1), 168–178.

Haase, D., Fink, J., Haase, G., Ruske, R., Pecsi, M., Richter, H., Altermann, M. & Jäger, K.D., 2007. Loess in Europe—its spatial distribution based on a European Loess Map, scale 1:2,500,000, *Quarter. Sci. Rev.,* **26**(9), 1301–1312.

Haesaerts, P., Borziak, I., Chirica, V., Damblon, F., Koulakovska, L. & Van der Plicht, J., 2003. The East-Carpathian loess record: a reference for the Middle and Late Pleniglacial stratigraphy in Central Europe, *Quaternaire,* **14**(3), 163–188.

Hatté, C. & Guiot, J., 2005. Palaeoprecipitation reconstruction by inverse modelling using the isotopic signal of loess organic matter: application to the Nußloch loess sequence (Rhine Valley, Germany), *Clim. Dyn.,* **25**(2–3), 315–327.

Hatté, C., Antoine, P., Fontugne, M., Rousseau, D.D., Tisnérat-Laborde, N. & Zöller, L., 1999. New chronology and eiranic matter δ13C paleoclimatic significance of Nußloch loess sequence (Rhine Valley, Germany), *Quarter. Int.,* **62**(1), 85–91.

Heller, F. & Evans, M.E., 1995. Loess magnetism, *Rev. Geophys.,* **32**(2), 211–240.

Heller, F. & Liu, T.S., 1982. Magnetostratigraphical dating of loess deposits in China, *Lett. Nat.,* **300,** 431–433.

Heller, F. & Liu, T.S., 1986. Palaeoclimatic and sedimentary history from magnetic susceptibility of loess in China, *Geophys. Res. Lett.,* **13**(11), 1169–1172.

Heller, G., Shen, C.D., Beer, J., Liu, X.M., Liu, T.S., Bronger, A., Suter, M. & Bonani, G., 1993. Quantitative estimations of pedogenic ferrimagnetic formation in Chinese loess and palaeoclimatic implications, *Earth planet. Sci. Lett.,* **114,** 385–390.

Hemming, S.R., 2004. Heinrich events: massive late Pleistocene detritus layers of the North Atlantic and their global climate imprint, *Rev. Geophys.,* **42**(1), doi:10.1029/2003RG000128.

Jordanova, D., Hus, J. & Geeraerts, R., 2007. Palaeoclimatic implications of the magnetic record from loess/palaeosol sequence Viatovo (NE Bulgaria), *Geophys. J. Int.,* **171**(3), 1036–1047.

Juvigné, E. & Semmel, A., 1981. Un tuf volcanique semblable à l'Eltviller Tuff dans les loess de Hesbaye et du Limbourg néerlandais, *Eiszeitalter und Gegenwart,* **31,** 83–90.

Kadereit, A., Kind, C.J. & Wagner, G.A., 2013. The chronological position of the Lohne Soil in the Nussloch loess section—re-evaluation for a European loess-marker horizon, *Quarter. Sci. Rev.,* **59,** 67–86.

Kimble, J., 2004. *Cryosols: Permafrost-Affected Soils,* Springer-Verlag.

King, J.W., Banerjee, S.K., Marvin, J.A. & Özdemir, Ö., 1982. A comparison of different magnetic methods for determining the relative grain size of magnetite in natural materials: some results from lake sediments, *Earth planet. Sci. Lett.,* **59,** 404–419.

Kukla, K., 1975. Loess stratigraphy of Central Europe, in *After the Australopithecines,* pp. 99–188, eds Butzer, K.W. & Isaac, G.L. Mouton, The Hague.

Lagroix, F. & Banerjee, S.K., 2002. Paleowind directions from the magnetic fabric of loess profiles in central Alaska, *Earth planet. Sci. Lett.,* **195**(1), 99–112.

Lagroix, F. & Banerjee, S.K., 2004a. Cryptic post-depositional reworking in aeolian sediments revealed by the anisotropy of magnetic susceptibility, *Earth planet. Sci. Lett.,* **224**(3–4), 453–459.

Lagroix, F. & Banerjee, S.K., 2004b. The regional and temporal significance of primary aeolian magnetic fabrics preserved in Alaskan loess, *Earth planet. Sci. Lett.,* **225**(3–4), 379–395.

Lang, A., Hatté, C., Rousseau, D.D., Antoine, P., Fontugne, M., Zöller, L. & Hambach, U., 2003. High-resolution chronologies for loess: comparing AMS ^{14}C and optical dating results, *Quarter. Sci. Rev.,* **22,** 953–959.

Lautridou, J.P., 1985. Le cycle périglaciaire pléistocène en Europe du Nord-Ouest et plus particulièrement en Normandie, *Thèse es Sciences,* Univ. Caen, Centre de Géomorphologie Caen, 908.

Liu, X.M., Hesse, P., Rolph, T. & Begét, J.E., 1999. Properties of magnetic mineralogy of Alaskan loess: evidence for pedogenesis, *Quarter. Int.,* **62**(1), 93–102.

Liu, Q.S., Deng, C., Torrent, J. & Zhu, R., 2007. Review of recent developments in mineral magnetism of the Chinese loess, *Quarter. Sci. Rev.,* **26**(3), 368–385.

Liu, Q.S., Banerjee, S.K., Jackson, M.J., Deng, C., Pan, Y. & Rixiang, Zhu, 2004. New insight into partial oxidation model of magnetites and thermal alteration of magnetic minerology of the Chinese loess in air, *Geophys. J. Int.,* **158,** 506–514.

Liu, Q.S., Roberts, A.P., Larrasoana, J.C., Banerjee, S.K., Guyodo, Y., Tauxe, L. & Oldfield, F., 2012. Environmental magnetism: principles and applications, *Rev. Geophys.,* **50,** RG4002, doi:10.1029/2012RG000393.

Maher, B.A., 2011. The magnetic properties of Quaternary aeolian dusts and sediments, and their palaeoclimatic significance, *Aeol. Res.,* **3**(2), 87–144.

Maher, B.A. & Thompson, R., 1991. Mineral magnetic record of the Chinese loess and paleosols, *Geology,* **19**(1), 3–6.

Maher, B.A., Thompson, R. & Zhou, L.P., 1994. Spatial and temporal reconstructions of changes in the Asian palaeomonsoon: a new mineral magnetic approach, *Earth planet. Sci. Lett.,* **125,** 461–471.

Maher, B.A., Prospero, J.M., Mackie, D., Gaiero, D., Hesse, P.P. & Balkanski, Y., 2010. Global connections between aeolian dust, climate and ocean biogeochemistry at the present day and at the last glacial maximum, *Earth-Sci. Rev.,* **99**(1), 61–97.

Marković, S.B. *et al.,* 2009. Middle and late Pleistocene loess sequences at Batajnica, Vojvodina, Serbia, *Quarter. Int.,* **198**(1), 255–266.

Marković, S.B. *et al.,* 2011. The last million years recorded at the Stari Slankamen (Northern Serbia) loess-palaeosol sequence: revised chronostratigraphy and long-term environmental trends, *Quarter. Sci. Rev.,* **30**(9), 1142–1154.

Matasova, G., Petrovsky, E., Jordanova, N., Zykina, V. & Kapicka, A., 2001. Magnetic study of Late Pleistocene loess/palaeosol sections from Siberia: palaeoenvironmental implications, *Geophys. J. Int.,* **147**(2), 367–380.

McManus, J.F., Oppo, D.W. & Cullen, J.L., 1999. A 0.5-million-year record of millennial-scale climate variability in the North Atlantic, *Science,* **183**(5404), 971–975.

Moine, O., Rousseau, D.D. & Antoine, P., 2005. Terrestrial molluscan records of Weichselian Lower to Middle Pleniglacial climatic changes from the Nussloch loess series (Rhine Valley, Germany): the impact of local factors, *Boreas,* **34**(3), 363–380.

Moine, O., Rousseau, D.D. & Antoine, P., 2008. The impact of Dansgaard–Oeschger cycles on the loessic environment and malacofauna of Nussloch (Germany) during the Upper Weichselian, *Quarter. Res.,* **70**(1), 91–104.

Nawrocki, J., Wojcik, A. & Bogucki, A., 1996. The magnetic susceptibility record in the Polish and western Ukrainian loess–palaeosol conditioned by palaeoclimate, *Boreas,* **25,** 161–169.

Necula, C., Panaiotu, C., Heslop, D. & Dimofte, D., 2013. Climatic control of magnetic granulometry in the Mircea Vodă loess/paleosol sequence (Dobrogea, Romania), *Quarter. Int.,* **293,** 5–14.

NGRIP, 2004. High-resolution record of Northern Hemisphere climate extending into the last interglacial period, *Nature,* **431,** 147–151.

Oches, E.A. & Banerjee, S.K., 1996. Rock-magnetic proxies of climate change from loess-paleosol sediments of the Czech Republic, *Stud. geophys. Geod.,* **40,** 287–300.

Orgeira, M.J., Egli, R. & Compagnucci, R.H., 2011. A quantitative model of magnetic enhancement in loessic soils, in *The Earth's Magnetic Interior,* pp. 361–397, Springer.

Özdemir, Ö., Dunlop, D.J. & Moskowitz, B.M., 1993. The effect of oxidation on the Verwey transition in magnetite, *Geophys. Res. Lett.,* **20**(16), 1671–1674.

Özdemir, Ö. & Dunlop, D.J., 1996. Thermal remanence and Néel Temperature of Goethite, *Geophys. Res. Lett.,* **23,** 921–924.

Özdemir, Ö., Dunlop, D.J. & Moskowitz, B.M., 2002. Changes in remanence, coercivity and domain state at low temperature in magnetite, *Earth planet. Sci. Lett.,* **194**(3), 343–358.

Özdemir, Ö., Dunlop, D.J. & Berquo, T.S., 2008. Morin transition in hematite: size dependence and thermal hysteresis, *Geochem. Geophys. Geosyst.,* **9,** Q10Z01, doi:10.1029/2008GC002110.

Özdemir, Ö. & Dunlop, D.J., 2010. Hallmarks of maghemitization in low-temperature remanence cycling of partially oxidized magnetite nanoparticles, *J. geophys. Res.: Solid Earth,* **115,** B02101, doi:10.1029/2009JB006756.

Panaiotu, C.G., Panaiotu, E.C., Grama, A. & Necula, C., 2001. Paleoclimatic record from a loess-paleosol profile in southeastern Romania, *Phys. Chem. Earth, Part A: Solid Earth Geod.,* **26**(11), 893–898.

Penn, R.L., Zhu, C., Xu, H. & Veblen, D.R., 2001. Iron oxide coatings on sand grains from the Atlantic coastal plain: high-resolution transmission electron microscopy characterization, *Geology,* **29**(9), 843–846.

Porter, S.C., Hallet, B., Wu, X. & An, Z., 2001. Dependence of near-surface magnetic susceptibility on dust accumulation rate and precipitation on the Chinese Loess Plateau, *Quarter. Res.,* **55**(3), 271–283.

Pouclet, A. & Juvigné, E., 2009. The Eltville Tephra, a late pleistocene widespread tephra layer in Germany, Belgium and Netherlands; symptomatic compositions of the minerals, *Geog. Belgica,* **12**(1–2), 93–103.

Rochette, P. & Fillion, G., 1989. Field and temperature behavior of remanence in synthetic goethite: paleomagnetic implications, *Geophys. Res. Lett.,* **16**(8), 851–854.

Rousseau, D.D. *et al.*, 2002. Abrupt millenial climatic changes from Nussloch (Germany) Upper Weichselian eolian records during the last glaciation. *Quarter. Sci. Rev.,* **21,** 1577–1582.

Rousseau, D.D., Sima, A., Antoine, P., Hatté, C., Lang, A. & Zöller, L., 2007. Link between European and North-Atlantic abrupt climate changes over the last glaciation, *Geophys. Res. Lett.,* **34,** L22713, doi:10.1029/2007GL031716.

Rowan, C.J., Roberts, A.P. & Broadbent, T., 2009. Reductive diagenesis, magnetite dissolution, greigite growth and paleomagnetic smoothing in marine sediments: a new view, *Earth planet. Sci. Lett.,* **277**(1), 223–235.

Sima, A. *et al.*, 2009. Imprint of North-Atlantic abrupt climate changes on western European loess deposits as viewed in a dust emission model, *Quater. Sci. Rev.,* **28,** 2851–2866.

Sima, A., Kageyama, M., Rousseau, D.D., Ramstein, G., Balkanski, Y., Antoine, P. & Hatté, C., 2013. Modeling dust emission response to North Atlantic millennial-scale climate variations from the perspective of East European MIS 3 loess deposits, *Clim. Past,* **9,** 1385–1402.

Spassov, S., Heller, F., Kretzschmar, R., Evans, M.E., Yue, L.P. & Nourgaliev, D.K., 2003. Detrital and pedogenic magnetic mineral phases in the loess/paleosol sequence at Lingtai (Central Chinese Loess Plateau), *Phys. Earth planet. Inter.,* **140**(4), 255–275.

Terhorst, B., Appel, E. & Werner, A., 2001. Palaeopedology and magnetic susceptibility of a loess–palaeosol sequence in southwest Germany, *Quarter. Int.,* **76,** 231–240.

Thompson, R. & Oldfield, F., 1986. *Environmental Magnetism,* Allen & Unwin, 227 pp.

Tissoux, H., Valladas, H., Voinchet, P., Reyss, J.L., Mercier, N., Falguères, C. & Antoine, P., 2010. OSL and ESR studies of Aeolian quartz from the Upper Pleistocene loess sequence of Nussloch (Germany), *Quarter. Geochronol.,* **5**(2), 131–136.

van Velzen, A.J. & Dekkers, M.J., 1999. Low-temperature oxidation of magnetite in loess-paleosol sequences: a correction of rock magnetic parameters, *Stud. geophys. Geod.,* **43**(4), 357–375.

Vandenberghe, J., 2013. Grain size of fine-grained windblown sediment: a powerful proxy for process identification, *Earth-Sci. Rev.,* **121,** 18–30.

Wang, X., Lu, H., Xu, H., Deng, C., Chen, T. & Wang, X., 2006. Magnetic properties of loess deposits on the northeastern Qinghai-Tibetan Plateau: palaeoclimatic implications for the Late Pleistocene, *Geophys. J. Int.,* **167**(3), 1138–1147.

Xu, W., Van der Voo, R., Peacor, D.R. & Beaubouef, R.T., 1997. Alteration and dissolution of fine-grained magnetite and its effects on magnetization of the ocean floor, *Earth planet. Sci. Lett.,* **151**(3), 279–288.

Zech, M., Rass, S., Buggle, B., Löscher, M. & Zöller, L., 2012. Reconstruction of the late Quaternary paleoenvironments of the Nussloch loess paleosol sequence, Germany, using n-alkane biomarkers, *Quarter. Res.,* **78**(2), 226–235.

Zhou, L.P., Oldfield, F., Wintle, A.G., Robinson, S.G. & Wang, J.T., 1990. Partly pedogenic origin of magnetic variations in Chinese loess, *Nature,* **346,** 737–739.

Zhu, R.X., Matasova, G., Kazansky, A., Zykina, V. & Sun, J.M., 2003. Rock magnetic record of the last glacial-interglacial cycle from Kurtak loess section, southern Siberia, *Geophys. J. Int.,* **152,** 335–343.

SUPPORTING INFORMATION

Additional Supporting Information may be found in the online version of this article:

Figure S1. Variations of a selection of magnetic parameters and ratios across the incipient tundra gley horizons IG5, IG6, IG8 and IG9. Their upper and lower boundaries as identified in the field (Antoine *et al.* 2009) are marked by dashed lines. Shaded horizons are the intervals over which redoxomorphic processes induced by waterlogging has left an imprint on the magnetic record (see discussion in Section 5.3) (http://gji.oxfordjournals.org/lookup/suppl/doi:10.1093/gji/ggu331/-/DC1).

Please note: Oxford University Press is not responsible for the content or functionality of any supporting materials supplied by the authors. Any queries (other than missing material) should be directed to the corresponding author for the article.
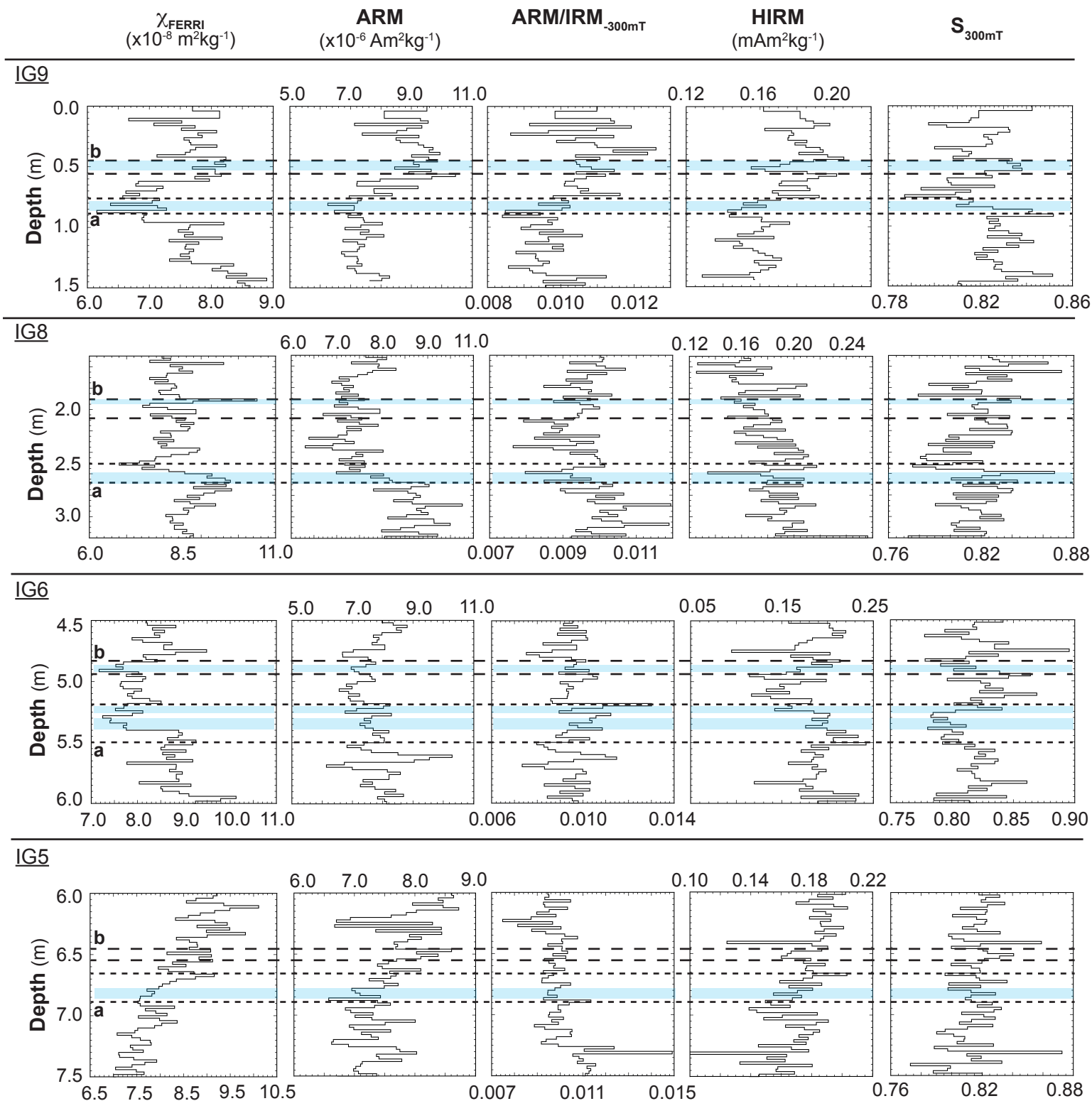
Supplemental Figure S1. Variations of a selection of magnetic parameters and ratios across the incipient tundra gley horizons IG5, IG6, IG8 and IG9. Their upper and lower boundaries as identified in the field (Antoine et al., 2009) are marked by dashed lines. Shaded horizons are the intervals over which redoxomorphic processes induced by waterlogging has left an imprint on the magnetic record (see discussion in section 5.3).